The Thesis Committee for Andrea Chengyi Chou
Certifies that this is the approved version of the following thesis:

Synthesis of Dibenzo[a,e]cyclooctatetraene based Conducting Polymer:

A Potential Molecular Polymer Actuator

APPROVED BY
SUPERVISING COMMITTEE:

Supervisor:

Bradley Holliday

Richard Jones

Synthesis of Dibenzo[a,e]cyclooctatetraene based Conducting Polymer:

A Potential Molecular Polymer Actuator

by

Andrea Chengyi Chou, B.S.

Thesis

Presented to the Faculty of the Graduate School of

The University of Texas at Austin

in Partial Fulfillment

of the Requirements

for the Degree of

Master of Arts

The University of Texas at Austin

December 2010

Acknowledgements

I would like to acknowledge the Holliday group for all their support and assistance in the experimental work.

<Dec. 3rd, 2010>

Abstract

Synthesis of Dibenzo[a,e]cyclooctatetraene based Conducting Polymer:

A Potential Molecular Polymer Actuator

Andrea Chengyi Chou, M.A.

The University of Texas at Austin, 2010

Supervisor: Bradley Holliday

A new polymer with dibenzo[a,e]cyclooctatetraene as the actuation center and one of the thiophene derivatives, 3,4-ethylenedioxythiophene, as polymer chain is successfully synthesized. Nuclear magnetic resonance spectrum is obtained for each synthetic step. Several electrochemistry tests are done to examine the oxidation and reduction properties of the monomer and polymer. Cyclic voltammetry is used for the polymerization. Polymer is first grown on a metallic working electrode and further coated on an ITO plate. UV-Vis experiment is also done. A $\pi \rightarrow \pi^*$ transition is observed as the primary polymer electronic absorption peak. Thickness of the polymer film is also recorded.

Table of Contents

List of Tables

List of Figures

Chapter 1: Introduction

Many scientists and doctors are looking for potential replacements for human skeletal muscle, which is a natural protein polymer with a combination of several essential and unique mechanical properties, such as active strain, power to mass ratio, different levels of stiffness, …etc.[1,2] Years ago, research scientists at the Jet Propulsion Laboratory in Pasadena, California started a new project to build a robotic arm using electroactive polymers.[3] Furthermore, earlier this year, Medical Center at University of California at Davis has announced that a group of their surgeons have found a way to help patients suffering from facial paralysis to restore their eyeblinking ability through an application of artificial muscle. This work is done with the usage of electroactive polymers as well.[4,5] This collective work shows that electroactive polymers and artificial muscles have become a more interesting and rapidly developing topic for researchers in many fields.

1.1 Artificial Muscle and Related Materials

1.1.1 History of Artificial Muscle and Electroactive Polymers

Electroactive polymers (EAP) has not been a topic with huge attraction for years due to limited capability in actuation and low availability of new materials in the past.[6] However, EAP materials have a stable ability to retain potential change and, in fact, EAP not only can induce the actuation strains needed for several applications but also has the ability to restore shape. In addition, EAP is

analogous to natural muscles. As more materials are made and examined to serve as a proper EAP, more scientists have increased their interest in this area and more focus is drawn to this new topic.[6,7]

In general, polymers are thought to be adequate replacements for muscle. Its linearity and deformation is similar to actual muscle movement. To activate a polymer deformation, many mechanisms are examined and reported in various literature work. Common activations reported are chemical, thermal, pneumatic, magnetic, optical, and electrical.[8-14] Polymer deformation due to chemical activation can be done by changing the chemical environment of the medium, for example, adding a small amount of acid or base can control a reversible shape alternation.[15] Changing the temperature affects the thermal expansion and can also deform both linear and nonlinear polymers.[16] Optical activation with photomechanical effect influences polymer contraction in volume which is initiated by light.[17] However, electrical activation is the most promising EAP stimulation.[9]

The history of EAP experiment can be traced back to the 19th century.[9] Röntgen had observed the shape change in a rubber band through electrical deformation in 1880.[18] This experiment was done with a natural rubber band with 1 m in length and 16 cm in width. Through charging and discharging, this rubber band could have a length differ by a few centimeters.[19] In 1899, Sacerdote did an experiment which formulated a polymer's strain response to an electric field

activation.[20] Furthermore, in 1925, a discovery of piezoelectric polymer by Eguchi opened a new era in EAP history. According to Eguchi, this piezoelectric polymer was named as "electret" and prepared with a mixture of carnauba wax, bees wax, and rosin.[21,22] Electrets are polymers in which the electric dipole moments align relative to each other.[18] The original electret made by Eguchi was permanently charged and still has a surface charge one-seventh of its original value 45 years ago. This electret is now preserved in Tokyo Science Museum.[22,23] Another big milestone for EAP history is contributed by Kawai in 1969 with the discovery of poly(vinylidene fluoride) polymer (PVDF or PVF2).[6] PVDF is a crystalline polymer. This material has demonstrated substantial piezoelectric activity and has four different phases. Because of this property, PVDF has a very board usage in EAP applications as a ferroelectric polymer.[6,24]

While the list of polymer materials being developed has grown since the 70's, the real progress in EAP research does not start until 1990. There are two categories of EAP materials: ionic and electronic.[9] These are further discussed in later sections.

1.1.2 Natural Muscle and Its Movements

The human body is composed with three major types of muscles – cardiac, smooth, and skeletal muscle. Cardiac muscle is found in heart. Smooth muscle is usually used as the muscles to form organs. Both cardiac and smooth muscles are

involuntary, i.e. these kinds of muscles are not under conscious control. Skeletal muscle (or skeleton muscle) is voluntary. It is anchored to bones through tendons and directly responsible for skeletal movements. Artificial muscle made these days is an analogy to skeleton muscle.[26]

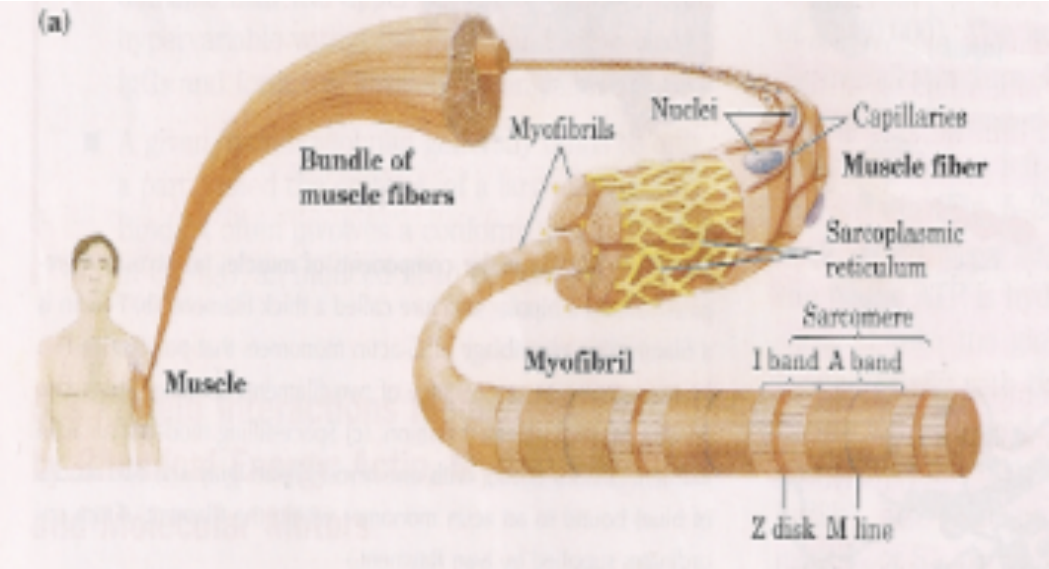

Figure 1: Structure of Skeleton Muscle.[27]

Muscles are made by myosin and actin. Molecules of myosin proteins compose thick filaments and multiple actin proteins become filamentous actin, which plays a major role in thin filaments along with other proteins like troponin and tropomyosin.[27] The movement unit of skeleton muscle is called a sarcomere, which starts from a Z-disk to another Z-disk. Z-disk is used as an attachment for a bundle of thin filaments to anchor (I-band) and I-band is bisected by Z-disk. Next to I-band are bundles of thick filaments called A-band and A-band is bisected by M-line. In other words, each sarcomere is composed of A-band and two half I-

bands with M-line as the center of sarcomere. Multiple sarcomeres then form a linear structure called myofibril. Myofibril is surrounded by sarcoplasmic reticulum and approximately a thousand combinations of myofibril with sarcoplasmic reticulum can make one muscle fiber. This fiber typically has diameter from 20 to 100 μm and each muscle is composed by bundles of muscle fibers.[27,28]

The movement of muscle happens at the sarcomere. Sarcomere must change in length during contraction and this contraction occurs while thick filaments slide along thin filaments. The contraction of a sarcomere is shown in *Figure 2*. During the contraction, I-band is compressed and A-band remains the same.[27,28]

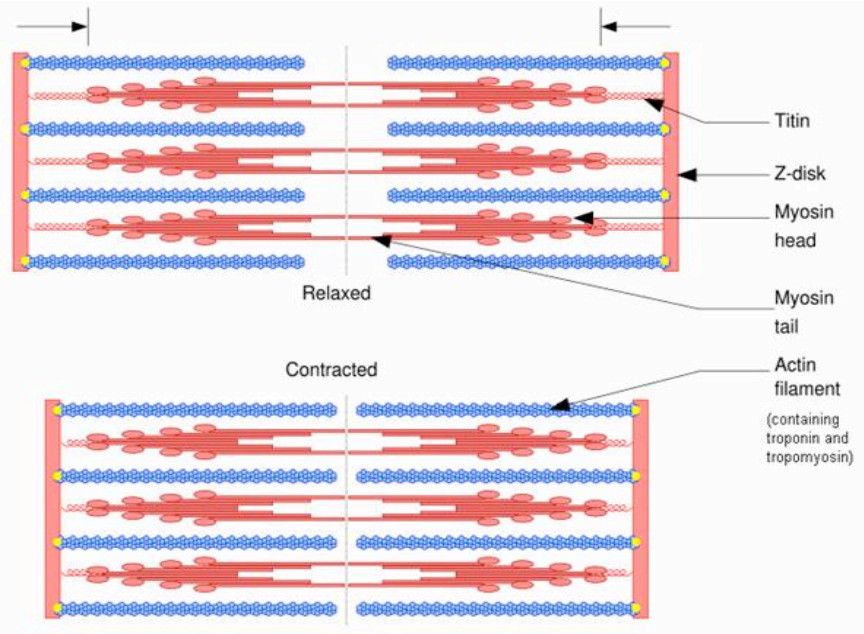

Figure 2: Muscle Contraction.[28]

The movement of muscle is a reversible process. In the first step, the myosin head that is connected to an actin site undergoes dissociation. This myosin head is now bound to ATP. Then, ATP is generated to form ADP and phosphate due to a hydrolysis. This hydrolysis causes the change in sarcomere conformation. Afterwards, the myosin head would bind to another site on the actin filament which forces both ADP and phosphate to be released. This initiates a "power pump" with myosin back to its original conformation as the I-band decreases. Each time, the sarcomere can generate a force of 3 to 4 pN. Moreover, relative to a thin filament, thick filaments can move about 5 to 10 nm.[27,29] *Figure 3* illustrates a simple expression of muscle movement mechanism.[29]

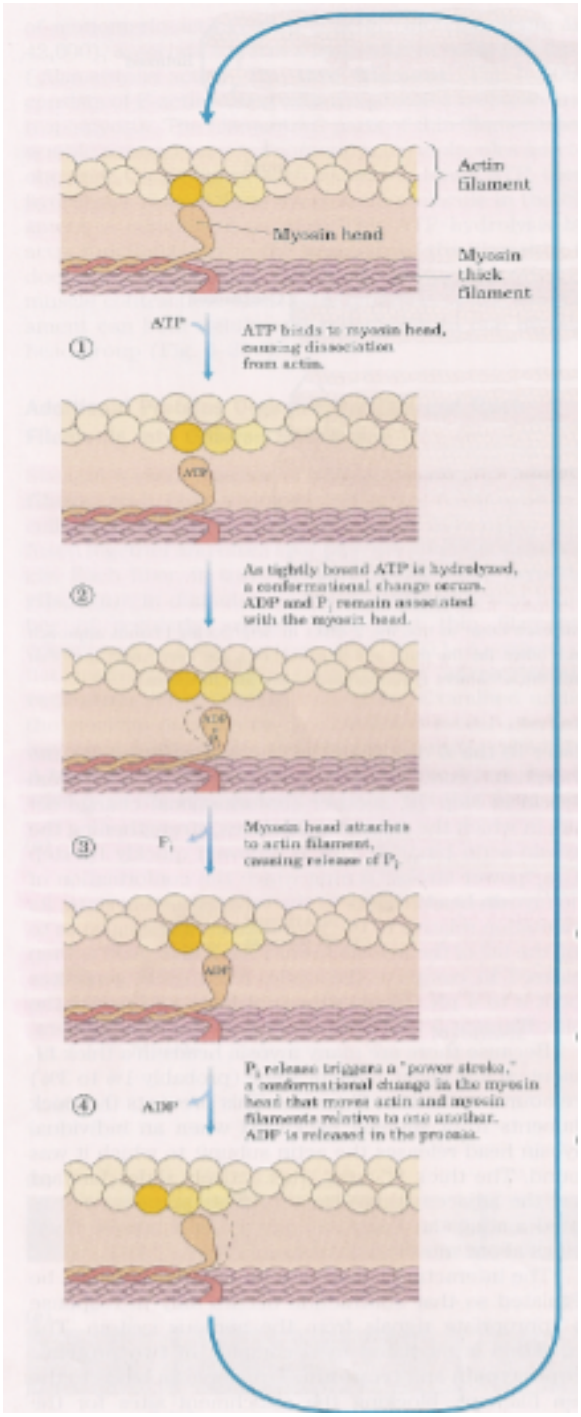

Figure 3: Myosin Action Model.[28]

Theoretically, either a linear motor or a rotary motor can serve as an actuation center in biological muscle movement system. However, the myosin and actin filaments in skeletal muscles function more like a linear motor. In order to create an artificial muscle which has properties similar to a skeletal muscle, an artificial muscle with linear motion would be a better option in terms of mimicking the skeletal muscle. For example, Collin *et al*. have designed a molecular shuttle system with rings. These rings can glide through the filament and hence the filament can be stretched and contracted electronically and photochemically.[30,31]

With the basic principles of muscle movements, researchers can design different types of artificial muscle and its precursors appropriately. In the next section, various types of artificial muscles are discussed.

1.2 Different Types of Artificial Muscles

To design a new generation of artificial muscle, we first need to study the current materials carefully. Materials that have served as appropriate candidates can be categorized in different groups. There are two major groups for polymer materials: electric polymers and ionic polymers.[32] According to Mirfahrai *et al*., each polymer can undergo a length or volume change based on different driven force. The actuation of an electric polymer is initiated by a change in electric field while the ionic polymer actuates according to a difference in ions.[1]

1.2.1 Electronic Artificial Muscle

Based on review written by Mirfakhrai, Wadden, and Baughman, electronic artificial muscle provides an easier mechanism for actuation.[1] This mechanism involves an interaction between the two electronic fields, such as electrodes and this would lead to an electrostatic interaction or piezoelectricity.[1,9] In general, this type of artificial muscle can obtain a large strain (up to approximately 7 %) and excellent work density.[1]

There are three major types of electronic artificial muscles: dielectric elastomer actuators, electrostrictive relaxor ferroelectric polymers, and liquid crystal elastomers. In the following sections, we will discuss each actuator type and respective applications.

1.2.1.a Dielectric Elastomer Actuator

Dielectric elastomers are the most broadly used actuator among all the current materials. These materials are utilized in devices with a layer of elastic dielectric film sandwiched by two compliant electrodes. When voltage is applied to the device, the opposite charges on the two electrodes attract which leads to a compression in the dielectric film. At the same time, the dielectric film would also undergo the same charge repulsion. This effect is known as Maxwell strain and causes the device to have a two dimensional change of elongation (*Figure 4*).[1]

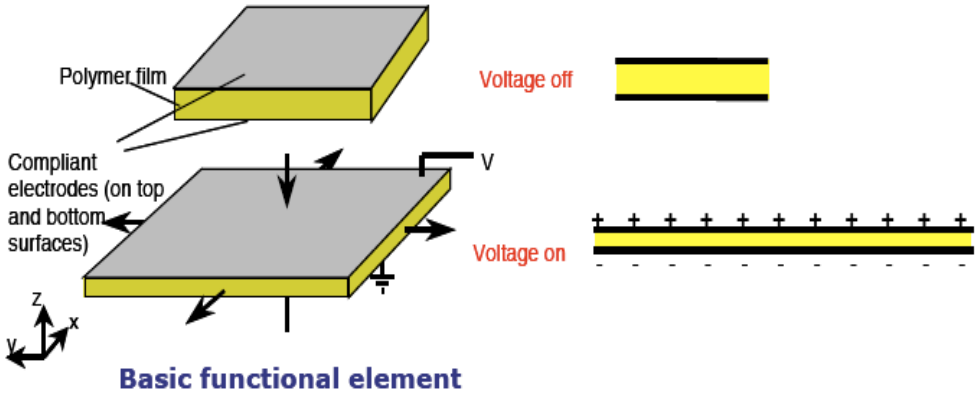

Figure 4: Actuation of a Dielectric Elastomer Actuator.[7]

This mechanism shows that dielectric elastomer actuator is able to convert electrical energy to mechanical energy.[7] The pressure which is induced by this mechanism can be calculated with formula 1.[7]

$$p = \varepsilon * \varepsilon_o * E^2 = \varepsilon * \varepsilon_o * (V/t)^2 \qquad (1)$$

In this formula, p is dielectric pressure, ε is dielectric constant of material, ε_o is the permittivity of free space, E is the imposed electric field, V is the applied voltage, and t is the thickness of polymer.[7,33]

Dielectric elastomer actuator is capable of generating large strains and strain rate (10 % ~ 100 %). The material used for the elastomer is usually silicone or an acrylic chemical coated with TiO_2 to increase the dielectric constant. For the electrodes, silver or conductive carbon is used and coated with conductive rubber or other materials.[1] Perline and coworkers have developed a new acrylic based polymer which can generate strain rate to 200%.[9,33] Devices using dielectric

elastomer actuator is widely applied in biomimetic robots (such as insect-like robots). It is also used as artificial muscles' in autofocus lens positioners.[1] However, the disadvantage of dielectric elastomer actuator is that it requires a large electric field (100 V/μm), which is a safety issue.[9]

1.2.1.b Electrostrictive Relaxor Ferroelectric Polymer

Ferroelectric materials are materials which possess dipole moments aligned relative to each other and in the same direction. These dipole moments of a ferroelectric material can be coupled with the material surface. Thus, if the charge on the surface is changed, the internal dipole of this material is also changed and hence the dimension of the material is also changed. In a ferroelectric polymer, this phenomenon can be achieved by alternating the conformation of the polymer materials.[1,25] When the electric field is changed, each monomer in the polymer also changes in order to fit the affect caused by the electric field. This influences the dimensional change of the polymer and is the origin of the electrostrictive relaxor ferroelectric polymer actuation.[1,9,25]

In general, inorganic ferroelectric materials can obtain a dimensional change of about 0.1%.[1] However, researchers have found a series of ferroelectric polymers which can increase the dimensional change to 10%.[1,9] This new series of polymers are coplymers of poly(vinylidene fluoride) (PVDF) and trifluoroethylene. Poly(vinylidene fluoride – trifluoroethylene), also known as

P(VDF-TrFE), can generate 4% electrostrictive strain between its nonpolar and polar regions.[9,25]

There is another type of electrostrictive polymer that is similar to the relaxor polymer. Electrostrictive relaxor polymer has a conformational change which initiates in the polymer backbone. Unlike the relaxor, this type of electrostrictive polymer has the polar groups incorporated as a side chain of the backbone. Therefore, the dimensional change occurs within the polymer due to the side chain, not the polymer backbone itself. This is called an electrostrictive graft polymer.[1] For a graft polymer, the backbone has to be very flexible and it has a smaller actuation rate due to the nature of the graft size.[1]

1.2.1.c Liquid Crystal Elastomer

Liquid crystal elastomer is a unique type of elastomer whose chemistry arises from its physical state – liquid crystal state, a state between liquid and solid crystal. For that reason, the orientation of each molecule inside the liquid crystal becomes essential while considering its chemical properties.[1,34] Liquid crystal elastomer, in most cases, is viewed as a rubber-like polymer and this rubber contains molecules whose orientations are ordered.[34] Since it is highly ordered, when an external influence is applied to the liquid crystal elastomer, the molerular orientation is affected and this increases the entropy of the system.[1,34,35] This is

also responsible for a molecular shape change which leads to the introduction of strains.[34,35]

The actuation mechanism for a liquid crystal material starts with a phase transition.[1,9,34,35] This transition can be easily initiated by an external stimulus such as light.[34] This actuation usually happens in an extremely short amount of time. The reverse actuation is slower than forward actuation but is still within 10 seconds.[9] Yet, the monomer still works more like a side chain and there are several points which would affect the usage of liquid crystal elastomer.[1,9] For example, the flexibility of polymer backbone, the cross-linking effect, and coupling between polymer backbone and liquid crystal groups are all important factors regarding the actuation mechanism.[9]

1.2.2 Ionic Artificial Muscle

Ionic artificial muscles are polymers whose actuation is done by an ion movement within the polymer corresponding to an applied field or a chemical reaction. This chemical reaction can be stimulation through electrons.[1,9] In that case, ions are still needed to balance the charge which is generated.[1] This type of artificial muscle requires low voltage from 1 to 7 V and a small electric field.[1,9] There are two principal ionic artificial muscles – carbon nanotube actuators (CNT actuators) and conducting polymers. Both materials require electrical stimulation.[1,9]

1.2.2.a Carbon Nanotube Actuator (CNT Actuator)

Carbon nanotube (CNT) is composed of pure carbon atoms and categorized as a carbon allotrope. It is also divided into two subgroups based on the way the CNT is folded. One is single-walled CNT (SWNT) and another is multiwalled CNT (MWNT).[1,35,36] SWNT is a CNT that can be analogous to a single rolled layer of graphite into a cylindrical tube (*Figure 5*).[1,35,37] SWNT can also be grouped based on its structural composition. Armchair, zigzag, and chiral SWNTs are shown in *Figure 6*.[35] MWNT, on the other hand, is a CNT that has multiple graphite layers. It is a nested system of SWNT.[1,35,36]

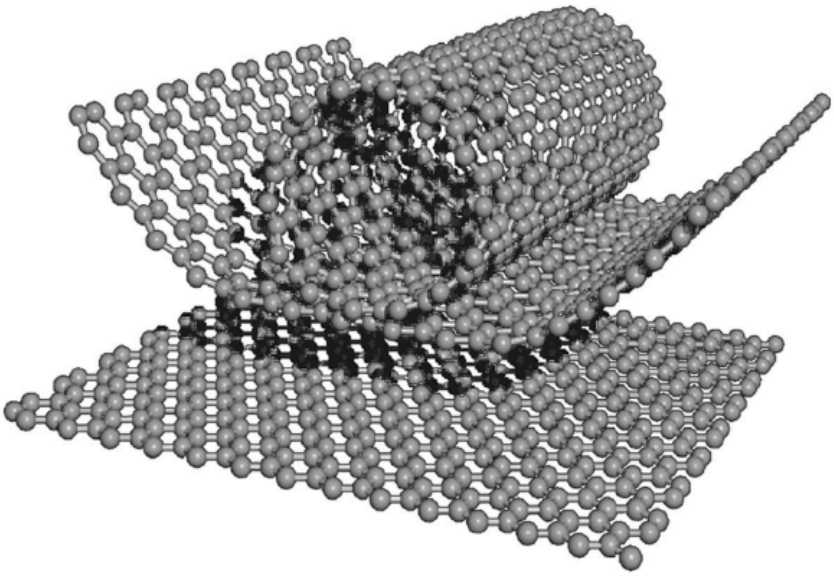

Figure 5: A Scheme of SWNT from a Single Graphite Layer.[37]

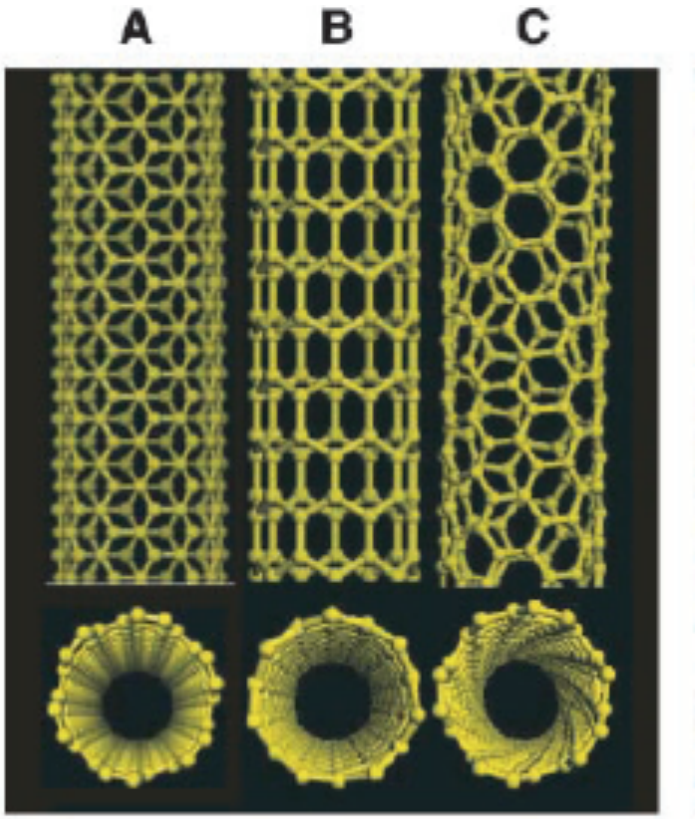

Figure 6: Different Types of SWNTs. (A) armchair, (B) zigzag, (C) chiral.[35]

The biggest advantage of CNTs is that it is very similar to skeleton muscles since it is viewed as an array of actuators.[36,38] The actuation of the CNTs is also electrostatic. Since CNT itself serves as its own electrode, when charge is applied to the CNTs in the same bundle, this CNT bundle would have the same charge spread out the entire surface area. This would lead to the same charge repulsion on the CNT bundle, which is strong enough to bend the stiff carbon-carbon bond, and hence the dimensional change is obtained.[1,36] However, because

of the stiffness of the carbon-carbon bond, CNT actuators can only provide low strain.[1]

1.2.2.b Conducting Polymer

Another key ionic polymer actuator is conducting polymer. Conducting polymer is, boardly, a series of organic polymer with the ability to conduct electricity.[39] This property makes conductive polymers work as semiconductors due to ion transfer along the polymer.[1] Moreover, this ion transfer is an ion insertion and deinsertion initiated by the change in the electric field.[1,9] The polymer goes through an oxidation-reduction reaction which is the origin of the change in dimension.[1,9,40] Typical conducting polymers used as an actuators are polypyrrole, polyaniline, and polythiophene (*Figure 7*).[1]

The actuation of a conducting polymer depends heavily on the electrolyte and the polymer structure because the structure can control the rate of actuation.[1] Generally speaking, conducting polymer actuators have a fast response rate which is good for an actuator.[40] Their low efficiency, however, requires some improvement.[9]

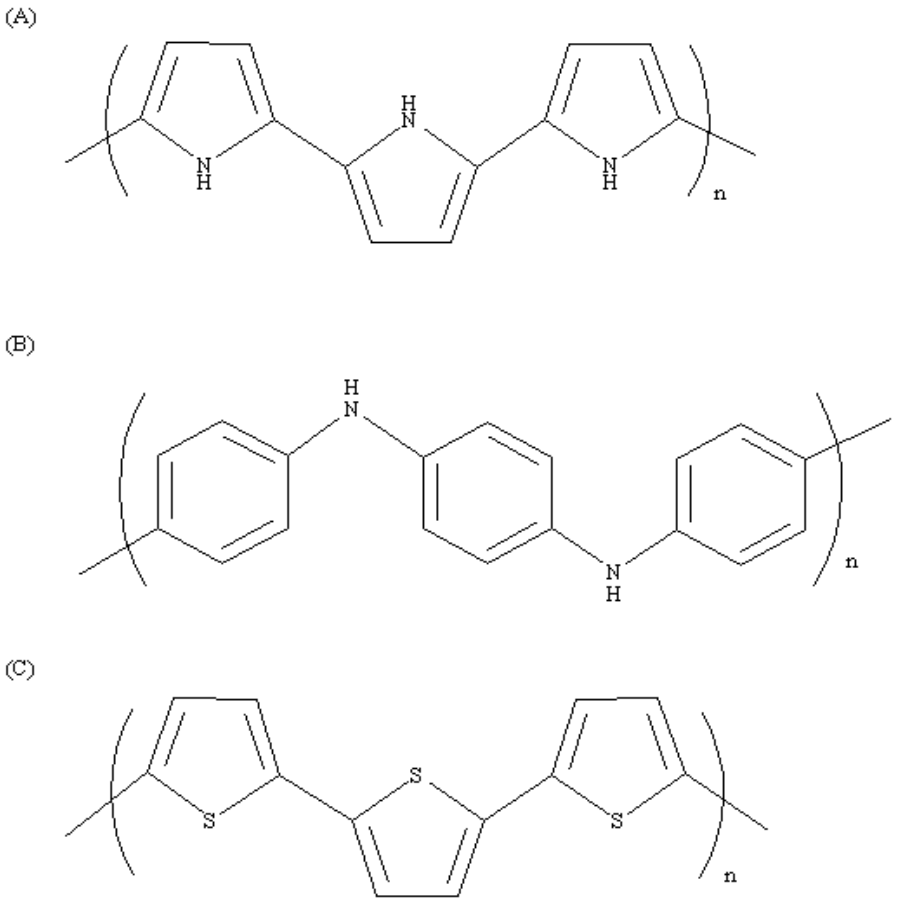

Figure 7: Common Conducting Polymers. (A) polypyrrole. (B) polyaniline. (C) polythiophene.

1.3 Conducting Polymer

Conducting polymers have become one of the popular materials for artificial muscles due to the ability to convert electrical energy into mechanical energy.[1,40] In addition to energy conversion, conductin polymers can also have

large change in volume.[1] Herein, a detailed study of conducting polymers is discussed.

1.3.1 History of Conducting Polymers

It is hard to say exactly who the first person to make a conducting polymer was and when it was prepared since many scientists have been working on making different precursors of conducting polymer for decades.[39] The related work can be traced back to the 19th century when Letheby published a paper with a successful synthesis of polyaniline by using aniline and an anodic oxidation.[39,41] However, according to Bott, these conducting polymers were mostly black powders and intractable.[42] These materials were difficult to analyze and characterize until Natta, who synthesized polyacetylene in 1950s, prepared black powers which were pure enough for a further characterization.[42]

The 1970s were the most remarkable era for this field of study.[39,42] Before the 1970s, the polymers synthesized were powder-like. In 1971, rather than powder, thin films of polymer were grown successfully on a wet surface.[42] Moreover, a new discovery provided a link between the redox reaction and the film's conductivity which illustrated that the conductivity of a polymer film could be increased to a metallic level with oxidation or reduction in 1976.[42] Last but not the least, in the 1970s, Alan J. Heeger, Alan, G. MacDiarmid, and Hideki Shirakawa devoted themselves to conducting polymer research and their work

was recognized with the Nobel Prize in 2000 "for the discovery and development of electronically conductive polymers."[39,43,44] In the 1990s, researchers such as Baughman and coworkers, Otero and coworkers, Della Santa, De Rossi and coworkers explored applications for conducting polymers in artificial muscles.[10,36,45-49] Conducting polymers have become a broadly discussed and salient chapter in chemistry.

1.3.2 Basic Principals of Conducting Polymer Operation

Currently, conducting polymers are still a conspicuous area of study for chemists. One reason is based on behavior of the polymeric system and another interest focuses on its application. Both fields of interest are noticed due to activity in electrochemistry.[39]

The properties of conducting polymers arise from an alternation between a carbon-carbon single bond and a carbon-carbon double bond.[39] The bond alternation can lead to a possible electron delocalization.[42] To explain this phenomenon, the nature of carbon is discussed. Carbon has four valence electrons. Two electrons are used to bind the adjacent carbon atoms and two σ bonds are formed. These σ bonds are connected and served as the backbone for the polymer. For the other two electrons, one is used to bind hydrogen and another would occupy the p_z orbital which ensures a π bond formation. This π bond is responsible for the electron delocalization. It is essential for the nature of

polymer characteristics.[39,42] *Figure 8* shows the simplest conducting polymer – polyacetylene.[39]

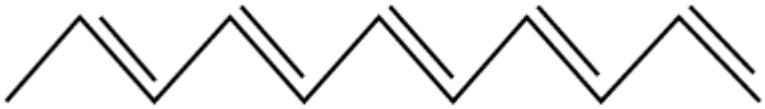

Figure 8: Structure of Polyacetylene.[39]

Conducting polymers are usually viewed as semiconductors, so a band gap is expected in a conducting polymer.[1,40] In fact, conducting polymers are conductive when doped with ions electrochemically or chemically.[1] To electrochemically control the conductivity, the oxidation level of the conducting polymer can be easily monitored. The electron conductivity represents the ability for an electron to travel through the polymer chain.[1,39] In order to possess a reversible electrochemical system, an anode, a cathode, and an electrolyte are required.[40] If a p-type dopant is introduced to the system, electrons are removed from the polymer and hence the polymer is oxidized. On the other hand, if an n-type dopant is added to the system, the polymer is reduced since the electrons are transferred from n dopant to the polymer.[39] Therefore, when adding cations or anions into the system, a polymer deformation would be observed.[40]

Generally speaking, a conducting polymer can bear a dimensional change because of the additional volume required for the charge compensating ion accommodation. This volume change usually happens due to the length change in

polymer.[40] When electrons are introduced or removed form the polymer, a polymeric shape change would occur simultaneously. Therefore, the orientation of the polymer chain is essential.[1,40] Also, the environment, i.e. electrolyte and solvent, has a significant influence on the conductivity.[1]

Chapter 2: A Potential New Polymer Actuator

In this research project, a new actuator with the ability to serve as a possible actuator for an artificial muscle is designed. This polymer has a backbone chain which containes 2,8-dibenzocyclooctatetraene (DBCOT) and 3,4-ethylenedioxythiophene (EDOT).

2.1 *2,8*-Dibenzocyclooctatetraene (DBCOT)

While designing a new monomer for a polymer backbone, the center of actuation is considered first. In this project, cyclooctatetraene (COT) is taken into consideration due to its two conformations: tub and planar.[50] COT has 8 π electrons. According to Huckel's rule, a monocyclic ring is aromatic and planar when it has 4n+2 π electrons.[51] Since 8 does not satisfy the 4n+2 rule, COT is not planar when it is neutral because it is anti-aromatic.[50,51] In fact, if 2 electrons can be removed from COT, the system would now have 6 π electrons and hence Huckel's rule is achieved and a planar conformation is observed.[52] Therefore, COT is selected as the unit of actuation since it has a simple structure and possess an ideal change in conformation, from tub to planar.[41,52] This conformation change is illustrated in *Figure 9*.[52] In this figure, it clearly explains that the conformation change is initiated by gaining or losing electrons. Moreover, by a redox reaction, the molecular distance is changed based on the corresponding conformation.[52]

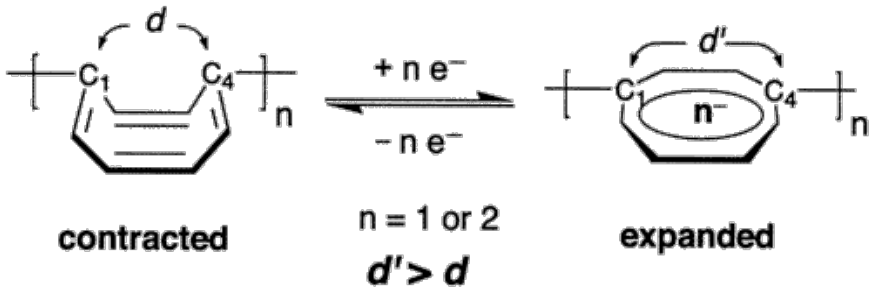

Figure 9: Scheme of Conformation Change for COT.[52]

This conformation change requires high activation energy. In other words, a slow electron transfer rate is expected during the process changing molecular geometry.[53] If 2 benzene rings are attached to the COT, these 2 rings would possibly affect the π electron delocalization in the planar transition state.[50] Based on the work done by Kojima *et al*. DBCOT provides a large change in structure on reduction.[53] DBCOT has a tub conformation with a point group of C_{2v} when neutral and a planar conformation with a point group of D_{2h} after undergoing a reduction of 2 electrons (*Figure 10*).[54,55]

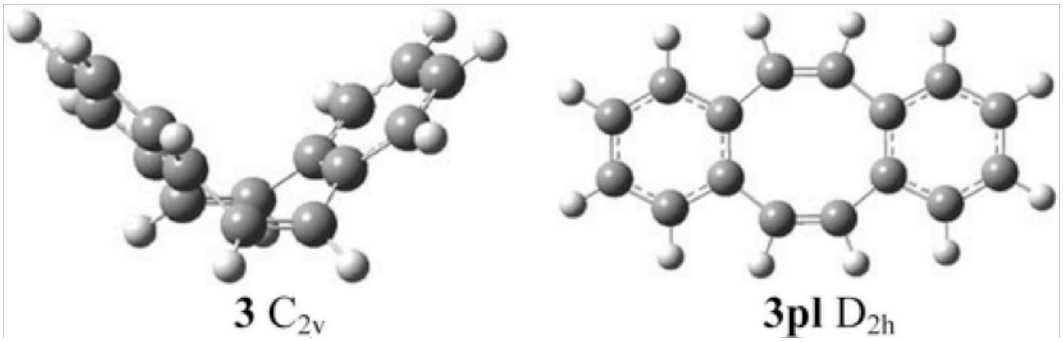

Figure 10: DBCOT Structure. Left: DBCOT, tub. Right: DBCOT, planar.[55]

2.2 Polythiophene and Derivatives

In 1977, Chiang and coworkers discovered that polyacetylene has a change in conductivity when the polymer is doped with Br_2, I_2, or AsF_5.[56,57] Several years later, polythiophene and corresponding derivatives were synthesized and studied.[57] For polymers like polythiophene, two possible structures are observed, which are aromatic and quinoid (*Figure 11*).[57,58] Additionally, the aromatic ground state and quinoid ground state have different energy states; in other words, they are not degenerate to each other.[57] Polythiophene, for example, has an aromatic ground state and a band gap which is associated with a change from the aromatic state to the quinoid state.[57]

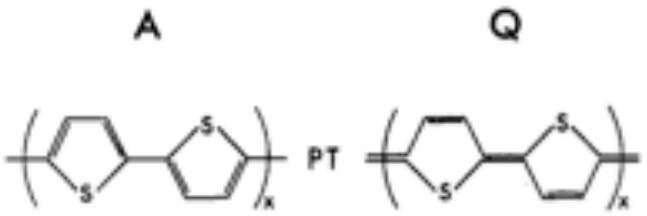

Figure 11: Structure of Polythiophene.[58]

Polythiophene usually can be synthesized by two methods: electrochemical or chemical.[59] The mechanism of polythiophene polymerization is shown as *Figure 12*.

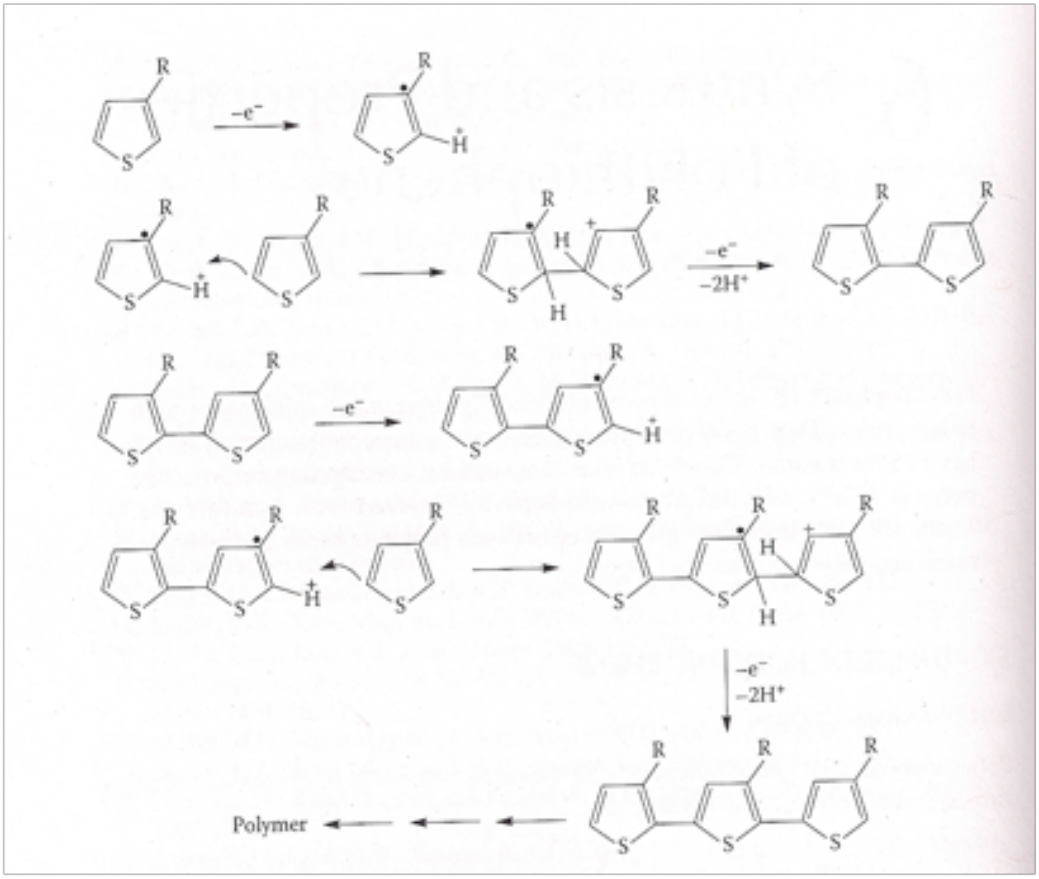

Figure 12: Mechanism of Polythiophene Synthesis.[59]

It is also noteworthy that there is an over-oxidation in the polythiophene polymer. This process can happen during the oxidative polymerization of the monomer when a constant current or a constant potential is applied.[59,60] This phenomenon can degrade the properties of polymer.[59] Such over-oxidation is shown as *Figure 13*.

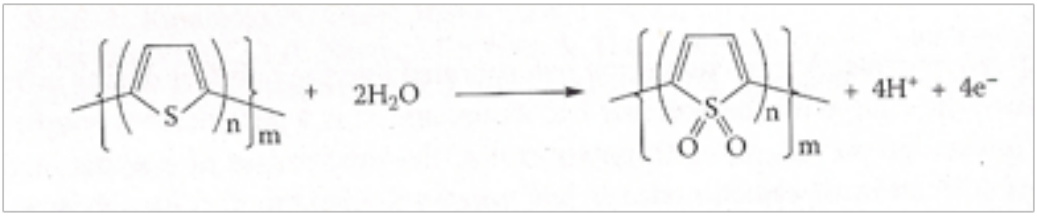

Figure 13: Over-Oxidation of Polythiophene.[59]

To decrease the over-oxidation in the polymer, the oxidation potential required for the polymerization needs to be decreased.[59] To do so, some scientists have used a bithiophene or terthiophene as the starting material when they perform the polymerization.[61] Other scientist have tried to minimize the oxidation potential by adding alkoxyl groups to the thiophene.[62] Both cases introduce a successful way to decrease the oxidation potential. Therefore, in this project, in order to obtain a new polymer, we design the starting material for polymerization as an EDOT monomer. The designed scheme for the monomer synthesis is illustrated in *Figure 14*.

2.3 Experimental

2.3.1 Synthesis

*5-Bromo-2-methylbenzaldehyde (***1***)*. To a three-necked round bottom flask with dry aluminum chloride (13.35 g) was added dry CH_2Cl_2 (37.5 mL). Suspension was stirred for 30 min. To the suspension was added *o*-tolualdehyde (7 g) slowly over 10 min. A solution of bromine (3 mL) and anhydrous CH_2Cl_2 (37.5 mL) was added slowly over 1.5 h. All addition was done at 0 °C under Argon. The

resulting suspension was allowed to bring back to room temperature and stirred under argon overnight. The suspension was poured into a beaker with crushed ice (125 g). The CH_2Cl_2 layer was separated and obtained. The aqueous layer was then extracted with CH_2Cl_2 three times. The combined organic layer was washed with 2 M HCl (three times), saturated $NaHCO_3$ (two times), $Na_2S_2O_3$ (once), and brine (once) respectively. The washed organic layer was dried with $NaSO_4$. Solvent was removed by rotavap and yielded a light orange oil. The oil was then diluted with hexanes (12.5 mL), cooled in -40 °C freezer overnight, and yielded a light yellow solid. The crude was warmly dissolved in hexanes (~25 mL) on a steam bath and decolorized with enough charcoal. The suspension was filtered and the clear colorless filtrate was cooled in -40 °C freezer again to yield a white solid (3.3675 g, 29.2 %).[63] ^{1}H NMR (300 MHz): δ 10.186 (s, 1H), 7.892 (d, 1H, *J*=2.1 Hz), 7.577 (dd, 1H, *J*=2.1, 8.4 Hz), 7.139 (d, 1H, *J*=8.4 Hz), 2.594 (s, 3H). ^{13}C NMR: δ 191.0, 139.3, 136.4, 135.5, 134.1, 133.5, 120.1, 18.9.

*(5-Bromo-2-methylphenyl)methylene Diacetate (***2***)*. To (**1**) (3.1924 g) was added acetic anhydrous (23.5 mL) and 4 drops of concentrated H_2SO_4. The yellow solution turned to a darker yellow color after the addition of H_2SO_4. The resulting solution was stirred overnight and poured into an Erlenmeyer flask with distilled water (~100 mL). The aqueous solution was extracted with EtOAc (three times). The combined organic layer was washed with saturated $NaHCO_3$ until neutral. The neutral solution is then washed with brine, dried over anhydrous $NaSO_4$, and

filtered to yield a pale yellow solution. The filtrate was rotavapped to yield a light yellow crystal (4.4481 g, 92.1 %). ^{1}H NMR (300 MHz): δ 7.741 (s, 1H), 7.609 (d, 1H, *J*=2.1 Hz), 7.397 (dd, 1H, *J*=2.1, 8.1 Hz), 7.053 (d, 1H, *J*=8.1 Hz), 2.365 (s, 3H), 2.105 (s, 6H). ^{13}C NMR: δ 168.6, 135.6, 135.2, 132.5, 132.4, 129.9, 119.6, 87.4, 20.7, 18.4.

*(5-Bromo-2-bromomethylphenyl)methylene Diacetate (***3***)*. To a mixture of (**2**) (4.0758 g), NBS (2.8913 g), and benzoyl peroxide (0.0324 g) was added DCE (40 mL). The suspension was stirred and refluxed for 3 h and cooled to room temperature. The solvent was removed by rotavap and a CH_2Cl_2 was added into the reslting yellow oily solution. The solution was washed by distilled water (three times), $Na_2S_2O_3$ (once), and brine (once) and dried over anhydrous Na_2SO_4. The solvent was removed by using rotavap and dried on Schlenk line to obtain a light yellowish orange crystal (4.6021 g, 89.5 %). ^{1}H NMR (300 MHz): δ 7.780 (s, 1H), 7.681 (d, 1H, *J*=1.8 Hz), 7.514 (dd, 1H, *J*=2.1, 8.4 Hz), 7.284 (d, 1H, *J*=8.1 Hz), 4.632 (s, 2H), 2.125 (s, 6H). ^{13}C NMR: δ 168.5, 135.7, 135.1, 133.3, 132.8, 131.4, 122.8, 87.4, 28.9, 20.8.

*(4-Bromo-2-diacetoxymethybenzyl)triphenylphosphonium Bromide (***4***)*. To a mixture of (**3**) (2.5051 g) and triphenylphosphine (1.7371 g) was added enough CH_2Cl_2 to dissolve the solid completely. The solution was stirred at room temperature over night. To obtain the crude, solvent was removed. The crude was then recrystallized with CH_2Cl_2 and ether to yield a beige powder (3.3205 g, 78.5

%). ^{1}H NMR (300 MHz): δ 7.612 (m, 19H), 5.633 (d, 2H, *J*=14.7 Hz), 1.904 (s, 6H).

*(5-Bromo-2-formylbenzyl)triphenylphosphonium Bromide (**5**)*. To a round bottom flask with (**4**) (2.0307 g) was added H_2O (50.0 mL) and 48 % HBr (10.0 mL). The suspension was stirred and refluxed for 8 h and cooled to RT. A milky yellow powder (1.3917 g, 81.5 %) was obtained after vacuum filtration and dried on Schlenk line for 2 d. ^{1}H NMR (300 MHz): δ 9.325 (s, 1H), 7.693 (m, 18H), 6.006 (d, 2H, *J*=15.9 Hz).

*2,8-Dibromodibenzo[a,e]cyclooctatetraene (**6**)*. This synthesis was carried under Argon. To a three neck round bottom flask with (**5**) (13.8248 g) was added 340 mL of absolute MeOH and refluxed. The NaOEt solution was prepared separately with solid NaH (0.6144) and absolute EtOH (35 mL). To the heated and refluxed MeOH solution was added the NaOEt solution dropwise over 3.5 h. A reddish orange drop was observed when NaOEt was added to the solution. The mixture was further refluxed for 1 h and cooled to RT. Vacuum filtration was used to separate the solid and solution. The solvent was removed via rotavap. A yellow crude was obtained and extracted with EtOAc and H_2O until no organic compound was found in the organic phase. The organic washes were combined, washed with brine, and dried over Na_2SO_4. Solvent was removed with rotavap and crude was dried on line. To purify the compound, column was run with pure hexanes. Crude was packed with silica gel and loaded to the column. All target

fractions were collected, combined, and solvent was removed with rotavap and then dried on Schlenk line to yield a white powder (0.6483 g, 7.0 %).[64] ^{1}H NMR (400 MHz): δ 7.282 (dd, 2H, *J*=2, 8.4 Hz), 7.183 (d, 2H, *J*=2 Hz), 6.905 (d, 2H, *J*=8.4 Hz), 6.662 (S, 4H). ^{13}C NMR: δ 138.8, 135.6, 133.2, 132.4, 131.7, 130.5, 130.1, 121.0.

*2,8-Di(3,4-ethylenedioxythiophene)dibenzo[a,e]cyclooctatetraene (**7**).* This synthesis was carried under Argon. To a round bottom flask was added (**7**) (0.2104 g), $PdCl_2(PPh_3)2$ (0.1181 g), CuI (0.0494 g), PPh_3 (0.0924 g), EDOT-$Sn(^{n}Bu)_3$ (0.0924 g) and dry DMF (35.0 mL). The mixture is heated to refluxed overnight. The suspension was added to NH_4Cl and H_2O relatively. CH_2Cl_2 was added to the aqueous suspension to extract the compound. The combined CH_2Cl_2 layers were washed with brine and dried over Na_2SO_4. Crude was obtained after solvent was removed by rotavap and dried on line. The compound was collected after column purification with CH_2Cl_2 and EtOAc until no impurity was found with TLC plate (0.0559 g, 19.9 %). ^{1}H NMR (300 MHz): δ 7.489 (dd, 2H, J=2.1, 8.1 Hz), 7.377 (d, 2H, *J*=1.5 Hz), 7.045 (d, 2H, *J*=8.4 Hz), 6.738, (s, 4H), 6.241 (s, 2H), 4.236 (m, 4H).

2.3.2. Synthesis Scheme

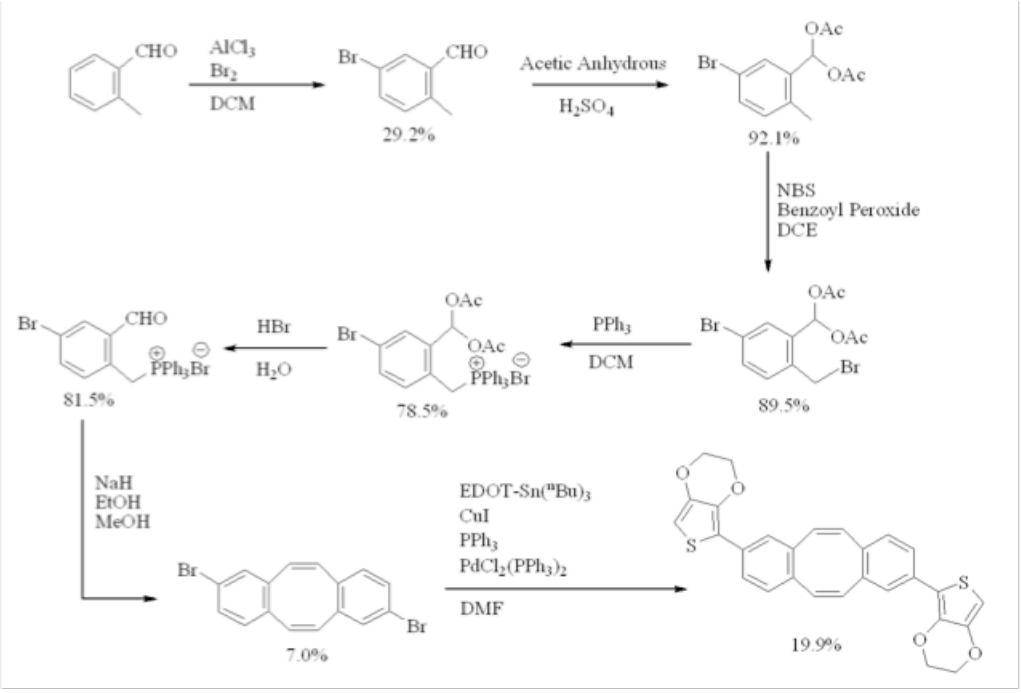

Figure 14: Scheme of the Monomer Synthesis.

2.4 Data Analysis

2.4.1 NMR Spectroscopy

All NMR spectra were done manually. Both ^{1}H NMR and ^{13}C $\{^{1}H\}$ NMR were run for each compound unless specified. All NMR spectra are attached in the appendix.

*5-Bromo-2-methylbenzaldehyde (**1**)*

In the ^{1}H NMR spectrum recorded for **1** (Appendix 1,2), there are 5 peaks that represent 5 proton groups in this molecule. The singlet peak at 10.186 ppm stands for the single proton in the aldehyde group. The singlet peak at 2.594 ppm

has three protons compared to other peaks and hence represents the methyl group. The aromatic region includes 3 peaks: small doublet at 7.892 ppm, doublet-doublet at 7.577 ppm, and large doublet at 7.139 ppm. This shows a pattern of protons on a 1,2,4-substituted benzene ring.

For the ^{13}C {^{1}H} NMR spectrum (Appendix 3), 8 peaks are observed which represents the 8 different carbons in this molecule. The aldehyde carbon is found at 191.116 ppm. In the aromatic region, 6 peaks are found which are the 6 carbons on the benzene ring. Three peaks are shorter because they are the three carbons which have no proton attached to them. Finally, the methyl carbon is found at 18.892 ppm.

*(5-Bromo-2-methylphenyl)methylene Diacetate (**2**).*

In the ^{1}H NMR spectra (Appendix 4,5), 6 peaks with a peak ratio of 1:1:1:1:3:6 from high to low ppm are observed. Compared to **1**, the aldehyde proton is gone in this case. Instead, a 6-proton-singlet peak at 2.105 ppm and a singlet of 1-proton-peak at 7.741 ppm are observed. These 2 peaks shows a successful replacement of diacetate group for the aldehyde.

This molecule has 10 different carbons. In the ^{13}C {^{1}H} NMR spectrum (Appendix 6), 10 peaks are found. The carbon at 191 ppm in **1** is gone and now observed at 87.417 ppm. In addition, the ester carbon at 168.558 ppm and a carbon at 20.749 ppm show the incorporation of the diacetate.

*(5-Bromo-2-bromomethylphenyl)methylene Diacetate (**3**).*

The ^{1}H NMR spectra (Appendix 7,8) of this molecule show a very similar pattern compared to **2**. Two major changes are observed. One is that the aromatic protons are deshielded. Another is that protons on the methyl group move from 2.4 ppm to 4.6 ppm and the peak intensity change from 3 protons to 2 protons. In its ^{13}C $\{^{1}H\}$ NMR (Appendix 9), 10 carbons are found. The most obvious difference is the carbon on the methyl now moves downfield from 18.4 ppm to 28.9 ppm due to the attached bromine.

*(4-Bromo-2-diacetoxymethybenzyl)triphenylphosphonium Bromide (**4**).*

The ^{1}H NMR spectrum (Appendix 10) shows two major differences compared to **3**. First, the aromatic region is now a mutiplet. This is because of the addition of 3 phenyl groups in which makes a total number of 19 aromatic protons in this molecule. Second, at 5.6 ppm, the 2 protons on the methyl group now changes from singlet to doublet due to the addition of triphenylphosphene. The triphenylphophonium group introduces $^{1}H - ^{31}P$ coupling and hence a doublet is observed.

*(5-Bromo-2-formylbenzyl)triphenylphosphonium Bromide (**5**).*

Like the ^{1}H NMR spectrum of **4**, this molecule's spectrum (Appendix 11) also shows a multiplet in aromatic region and a doublet at 6.0 ppm. The only change in this spectrum is the existence of a singlet at 9.325 ppm, which represents the successful conversion from diacetate to an aldehyde.

*2,8-Dibromodibenzo[a,e]cyclooctatetraene (**6**).*

For this molecule, a clean ^{1}H NMR spectrum is obtained (Appendix 12). This molecule has a C_{2v} symmetry and hence each proton has an identical proton in the same molecule. Therefore, there are only 5 groups of protons instead of 10 groups. The phenyl protons still give the pattern for a 1,2,4-substituted benzene: small doublet at 7.183 ppm, large doublet at 6.905 ppm, and doublet-doublet at 7.283 ppm. However, instead of 2 doublet peaks should be provided by the 4 protons on the cyclooctatetraene, a 4-proton-singlet is observed. The possible explanation for this observation is that the break in symmetry (– Br) is well removed from these protons which can make the 4 protons identical. Therefore, a 4-proton-singlet is showed on the spectrum rather than 2 2-proton-singlets.

Due to the symmetry, there are only 8 types of carbons in this molecule. In the ^{13}C $\{^{1}H\}$ NMR spectrum (Appendix 13), 8 carbon peaks are observed. Three of them have a shorter peak height since there are 3 quanternary carbons. All peaks are in the aromatic carbon region.

*2,8-Di(3,4-ethylenedioxythiophene)dibenzo[a,e]cyclooctatetraene (**7**).*

This molecule shows a similar ^{1}H NMR spectrum (Appendix 14,15) as **6** but more deshielded. The presence of two extra peaks is consistent with successful substitution of EDOT: an 2-proton-singlet at 6.241 ppm and an 8-proton-multiplet at 4.236 ppm. The same symmetry assignments are applied in this molecule. A proton ratio of 1:1:1:2:1:4 from low field to high field is obtained.

2.4.2 Electrochemistry

Polymerization of thiophene can be done electrochemically or chemically. In this case, the polymerization is done electrochemically. To initiate the polymerization, the monomer is oxidized first. One electron is removed and the monomer and is now a positively charged radical. A second equivalent of the monomer can now react with the radical cation to form a chain. This process can be done multiple times until the applied voltage in the system is stopped.[57,59]

In this project, the polymerization and electrochemistry was done in the glove box under nitrogen with moisture free conditions using *Gpes programming*. The polymer was grown in 0.1 M of $TBAPF_6$ in CH_2Cl_2 with small amount of monomer. The polymer was grown on a clean ITO plate after testing on metallic (Pf) working electrodes. The ITO plate coated with polymer was then retained for further analysis. Two solutions were prepared and used for analysis: 0.1 M $TBAPF_6$ in CH_2Cl_2 and 0.1 M $TBAPF_6$ in ACN.

0.1M $TBAPF_6$ in CH_2Cl_2 on ITO Plate

Most of the electrochemistry tests are done using this solution. *Figure 15* shows one of the polymerization experiments using this solvent.

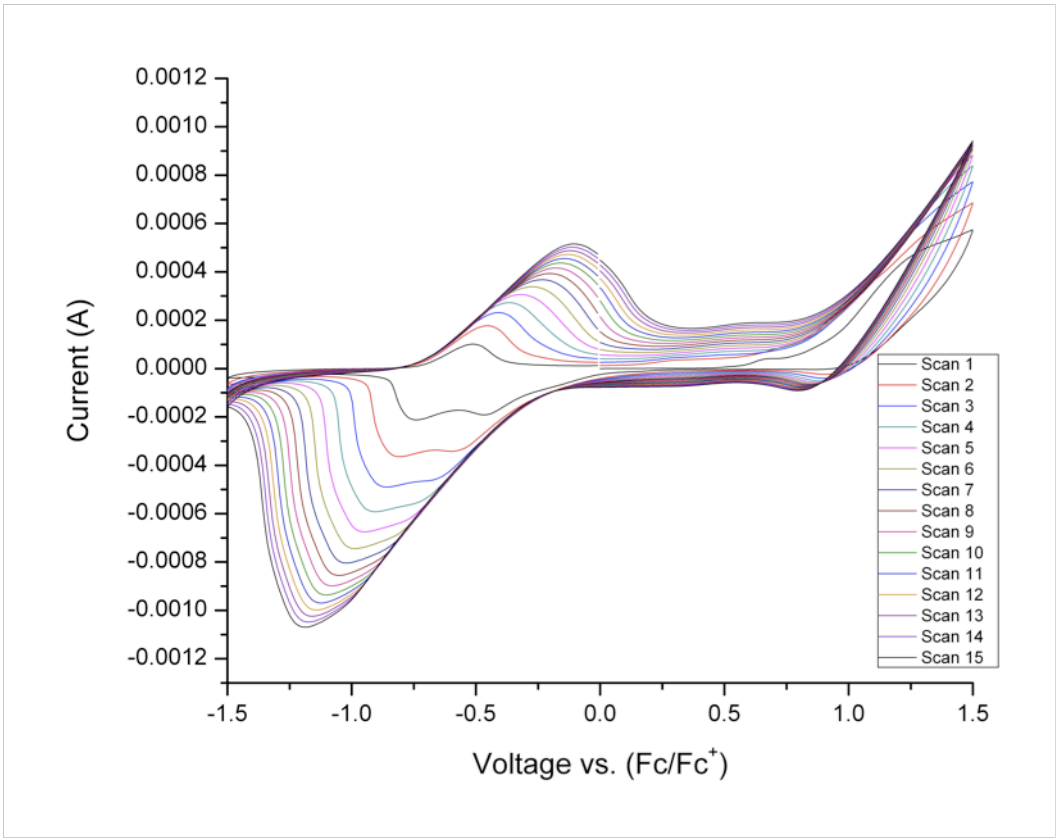

Figure 15: Electrochemistry Data using CH_2Cl_2 as solvent, Exp 1.

In this experiment, three ITO plates were used to grow three different plates using the same monomer solution. Fifteen scans were used for all three plates with a scan rate of 0.1 V/s and a step potential of 0.01 V. *Figure 15* illustrates the polymerization on plate 1. The number of scans is related to the amount of current that is running through the system. Ideally, the greater the number of scans is, the greater the current for the oxidation is, and therefore the thicker the film. In this case, there are three major peaks on this graph. One reduction peak is obtained at -1.2 V. Two oxidation peaks are found at 1.5 V and -0.2 V. All three plates have

the same oxidation/reduction peaks at the very similar voltage value (Appendix 16 – 18). With all the current values, a current vs. number of scans graph can be plotted for all peaks (*Figure 16 – 18*). Larger graphs are also attached in Appendix (Appendix 19 – 21).

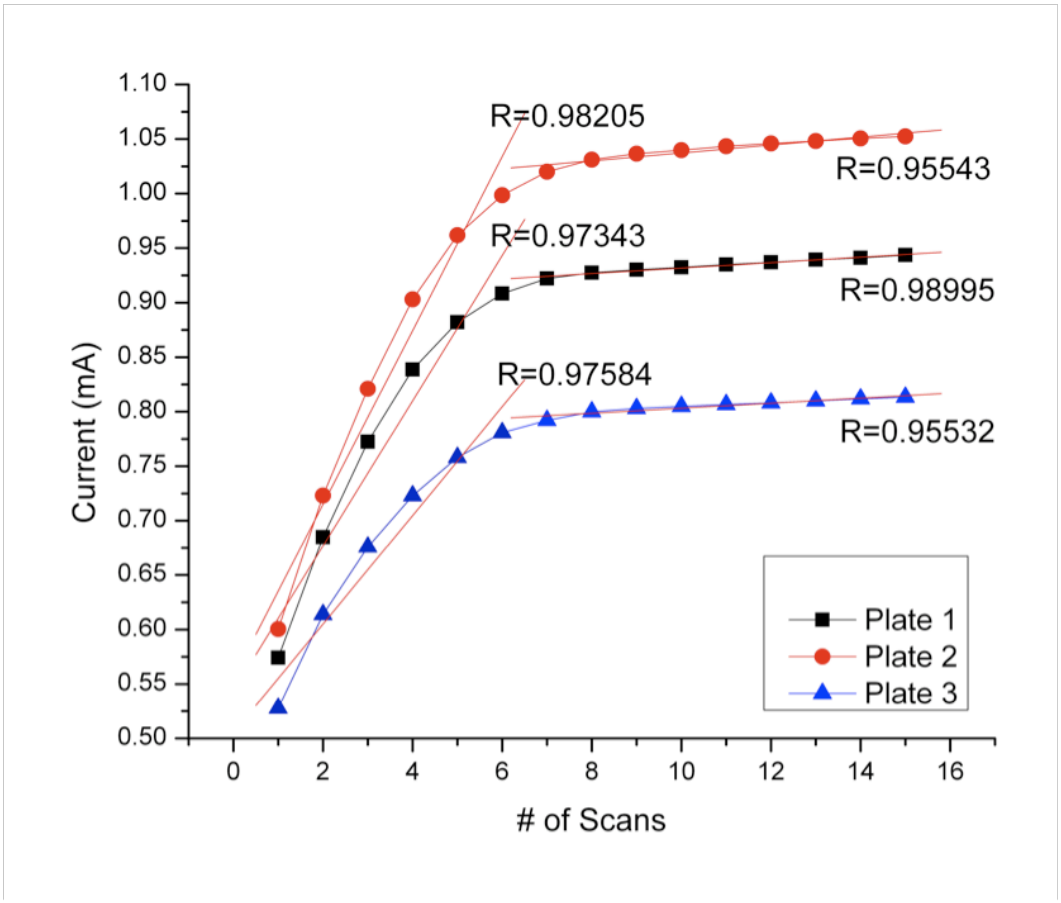

Figure 16: Current vs. Number of Scans for First Oxidation Peak (1.5 V).

In *Figure 16*, it is very clear that the film growth stops after the first seven scans. After the 8th scan, the data plot starts to flatten out. This shows that the polymerization of the monomer reaches a maximum at the 7th scan. After that, the

film might still be grown but at a much slower rate. To improve film groath, a better solvent is needed since the oxidation of the monomer can be over 1.5 V, which is the upper solvent window for CH_2Cl_2. *Figure 17* and *Figure 18* show that the redox property of the polymer is acceptable since the R values are very close to 1 and -1.

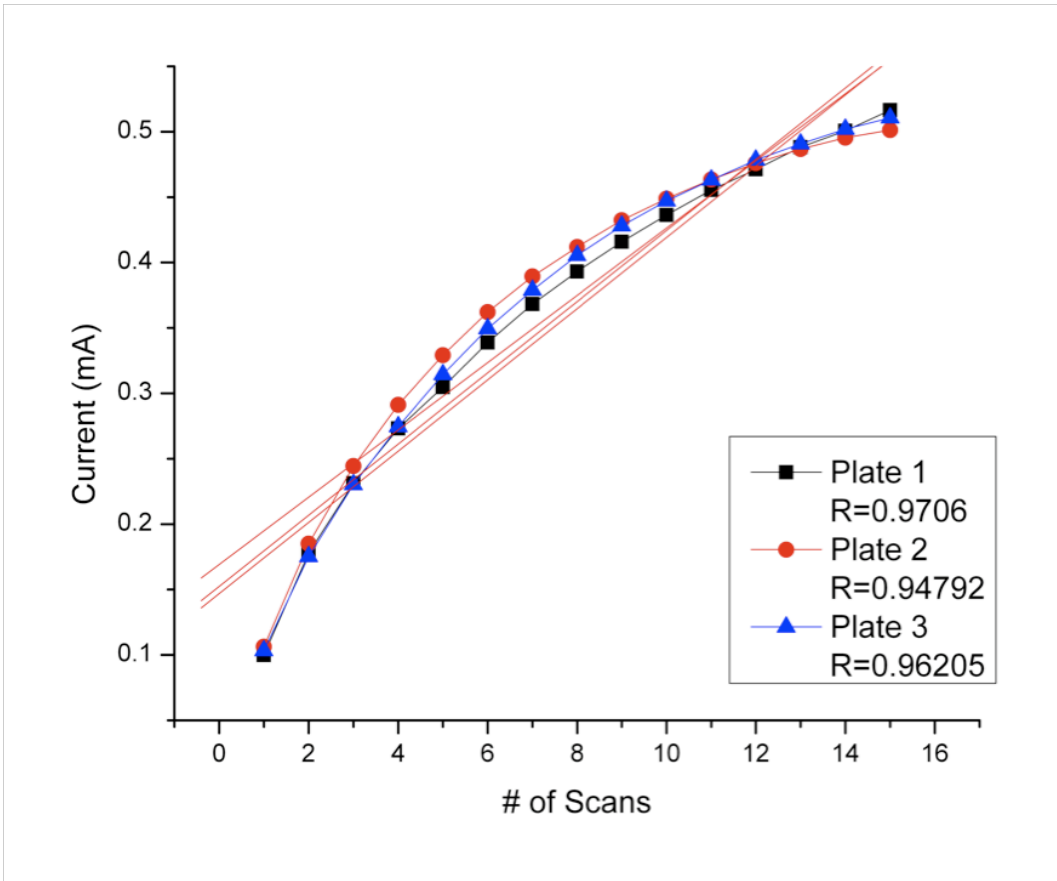

Figure 17: Current vs. Number of Scans for Second Oxidation Peak (-0.2 V).

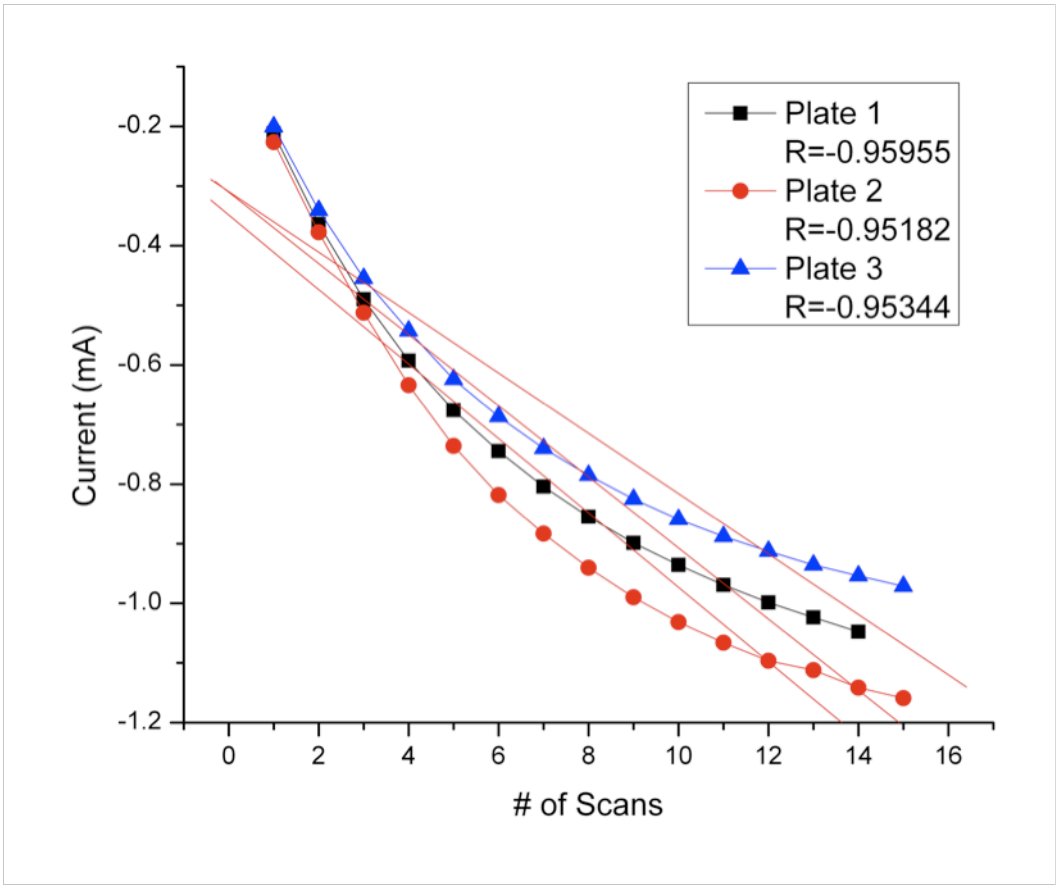

Figure 18: Current vs. Number of Scans for Reduction Peak (-1.2 V).

Once the film is obtained, a scan rate dependence test is run for each plate. The greater the scan rate is, the larger the current is obtained. *Figure 19* illustrates the relationship between current and the scan rate. The scan rate dependence is done with 3 scans for each trial and 0.01 V as the step potential. The scan rate examined values are 500, 250, 100, 50, 25, and 10 mV/s.

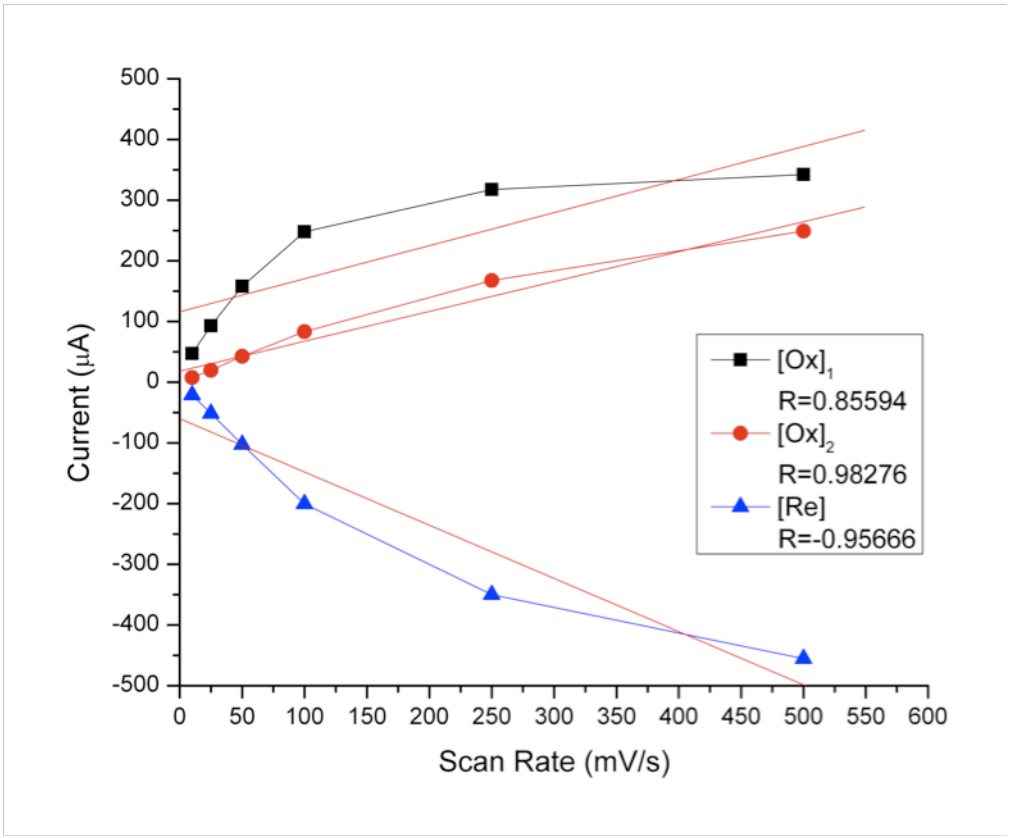

Figure 19: Current vs. Scan Rate for Plate 1.

In addition, the thickness of each film grown is recorded. Plate 1 has a thickness of 450 nm and 1000 nm at different locations on the film. Plate 2 has a thickness of 430 nm. Plate 3, however, has a thickness of only 230 nm. The possible explanation for this observation is that the film is not uniformly formed.

0.1 M $TBAPF_6$ in CH_2Cl_2 and ACN on Working Electrode

Since the previous experiment suggests that a solvent with a larger window is needed for the polymerization, ACN is selected as the solvent of interest since pure ACN can increase the voltage window from -2.5 V to 2.5 V.

The polymer was grown on the working electrode in 0.1 M $TBAPF_6$ in CH_2Cl_2 with small amount of monomer. The working electrode was washed with the corresponding electrolyte solution before the scan rate dependence test. Two working electrodes were prepared under identical conditions.

The voltage window selected for ACN was -2 V to 2 V after the ferrocene scan test. *Figure 20* shows the results for the scan rate dependence of the two solutions. First thing to notice is that the ACN sample has two smaller peaks around 0 V. These peaks come from the ferrocene test and the working electrode is not washed properly and hence small amount of ferrocene is attached to the bottom of working electrode. These peaks can be neglected in analysis. After measuring the current for oxidation and reduction, the scan rate dependence plot is shown in *Figure 21*. It is found that the ACN solution does give an overall better redox response than CH_2Cl_2 since both the oxidation and reduction give R values very close to 1 and -1. However, the monomer is not very soluble in ACN so the polymerization can not be accomplished in the ACN solution. Moreover, if a higher voltage is applied to the system, it is possible for the polymer to decompose.

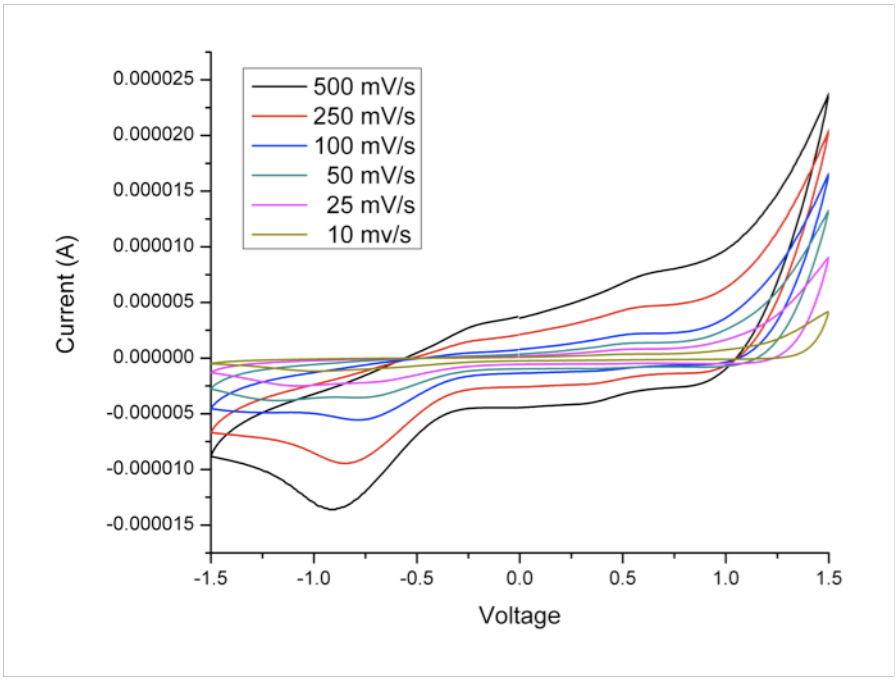

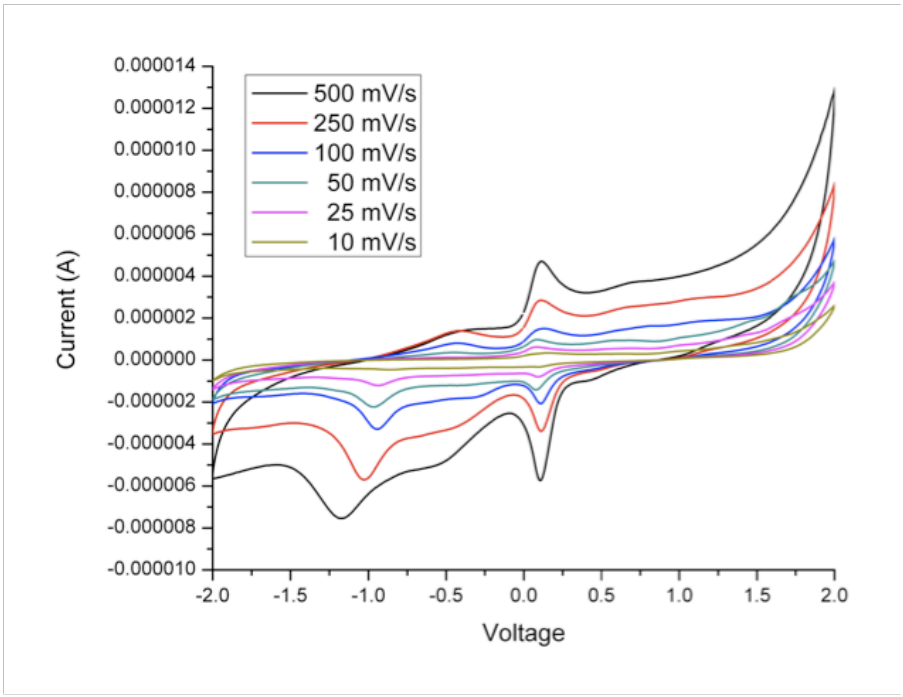

Figure 20: Current vs. Voltage for CH_2Cl_2 (top) and ACN (bottom).

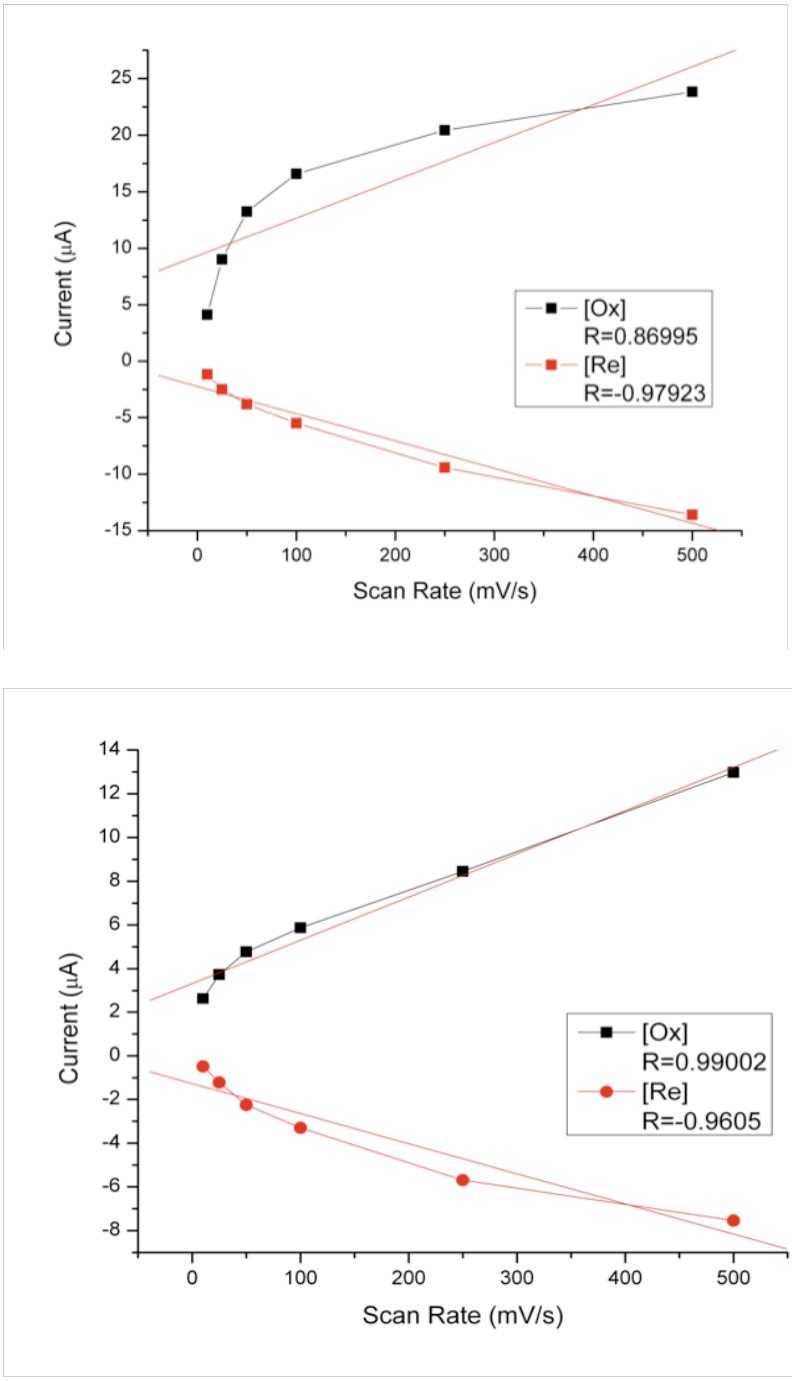

Figure 21: Current vs. Scan Rate for CH_2Cl_2 (top) and ACN (bottom).

Number of Scans vs. Thickness

To understand if the number of scans can influence the thickness of the film, an experiment is designed. All ITO plates were cleaned and four sets of solutions were prepared. The electrolyte solution was 0.1 M $TBAPF_6$ in CH_2Cl_2. The concentration of monomer in the electrolyte was 0.001 M. Four ITO plates were run under different number of scans: plate A and plate D were run under the identical conditions with 15 scans. Plate B was run with 30 scans and plate C with 45 scans. The thickness results were not ideal. Plate A had a thickness of 1100 nm. Plate B, however, had three different thickness readings of 1200, 600, and 200 nm. Plate C and plate D both had a thickness values around 200 nm.

It is possible to obtain multiple values for the same plate since the thickness measurement is done with different areas. However, due to this reason, a conductivity test can not be done if the thickness of the film is not uniform since conductivity is related to the film thickness.

2.4.3 UV-Vis Spectroscopy

A solution UV-Vis experiment was done for the EDOT monomer and a film UV-Vis measurement was done for the polymer film. UV-Vis data for the monomer is shown in *Figure 22*.

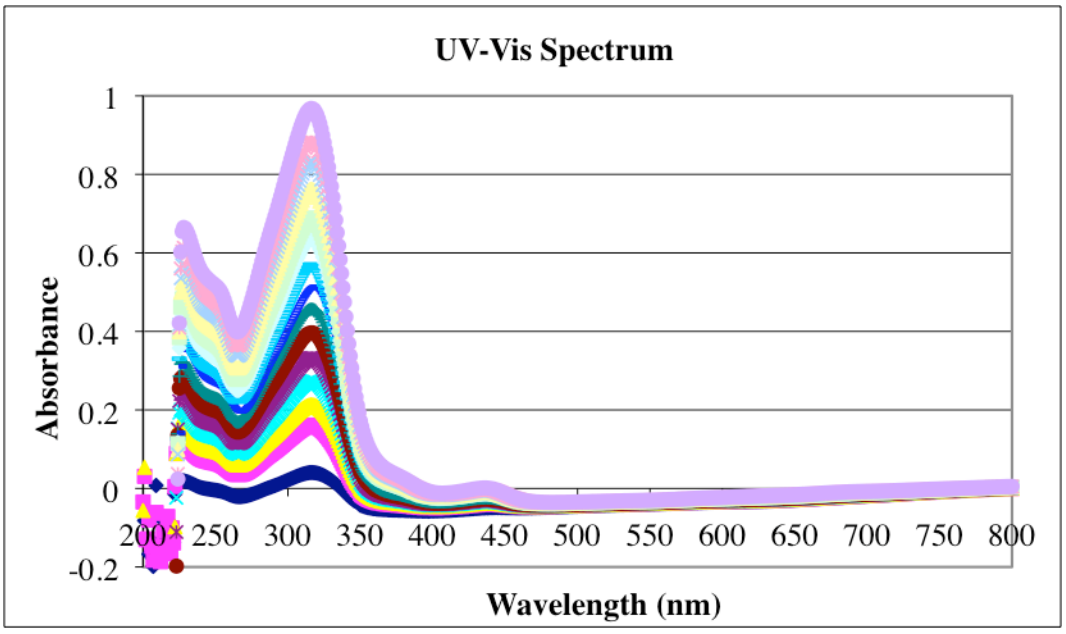

Figure 22: UV-Vis Absorption Spectrum for EDOT Monomer – Absorbance vs. Wavelength.

To perform a monomer UV-Vis absorption experiment, a small amount of monomer (10 mg) was dissolved in CH_2Cl_2 (10 mL) and the concentration of this stock monomer solution was calculated (2.064 mM.) Then, 3 mL of CH_2Cl_2 was added into the cuvette as the blank solution and the baseline was collected. Afterwards, 5 μL of the stock solution was added into the cuvette until a peak was obtained on the absorbance vs. wavelength graph. After a peak was found, 2 μL of the stock solution was added for each trial until the absorbance value reached 1. The absorbance data was then collected and molar absorptivity of each peak value was calculated by using Beer's Law shown in equation 2:

$$A = \varepsilon l c \qquad (2)$$

In *Equation 2*, *A* is absorbance; ε is molar absorptivity; *l* is path length, which is 1 cm in this case; *c* is concentration of the examined solution. The molar absorptivity was equal to absorbance divided by the path length and the sample concentration. The converted UV-Vis spectrum is showed in *Figure 23*.

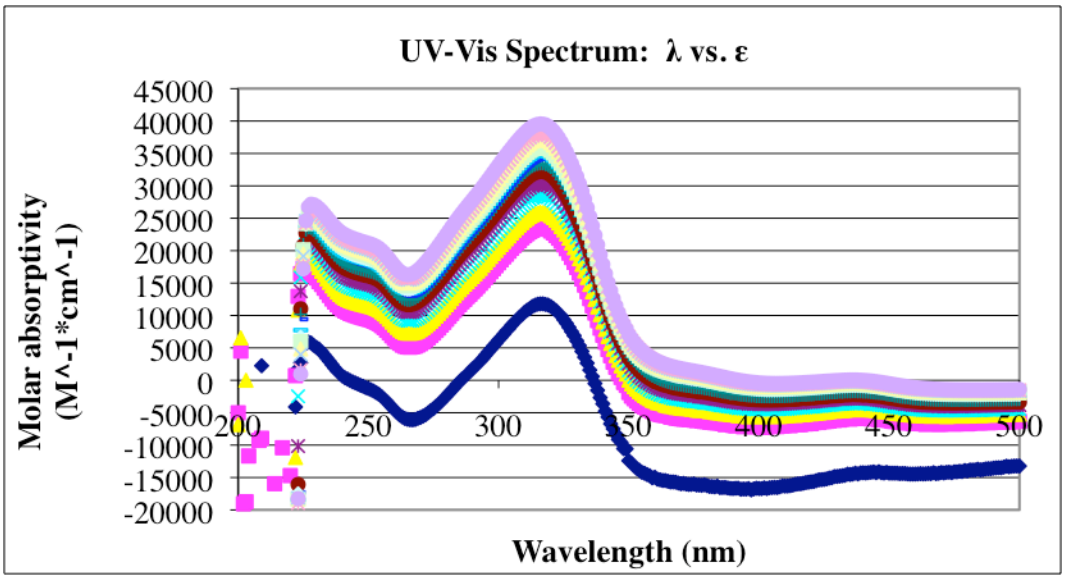

Figure 23: UV-Vis Absorption Spectrum for Monomer – Molar Absorptivity vs. Wavelength.

From *Figure 22*, four peaks are observed. Peak at 316 nm has the strongest absorbance. Peak at 227 nm also gives a relatively strong absorbance. At 256 nm, there is a shoulder observed. Finally, at 436 nm, there is a peak with very low absorbance.

The films used in this experiment are the polymers synthesized on plates 1, 2, and 3 from the electrochemistry experiment. The blank, or the baseline, of this experiment is made with two clean ITO plates. *Figure 24* shows that there are

three peaks observed. Peaks at 248 nm and 320 nm have an intense absorbance compared to the peak at 515 nm.

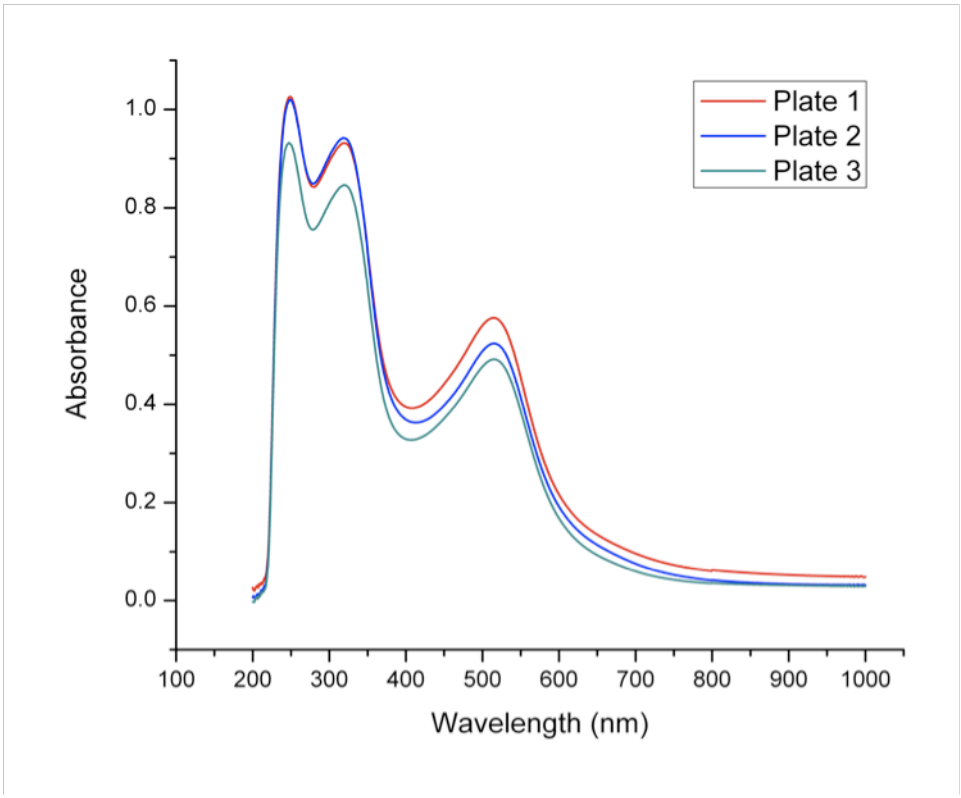

Figure 24: UV-Vis Absorption Spectrum for the Polymer – Absorbance vs. Wavelength.

A comparison in wavelength values among the DBCOT, monomer, and polymer is listed in *Table 1*.

Table 1: UV-Vis Wavelength Values for DBCOT, Monomer, and Polymer.

	Wavelength (nm)			
DBCOT[65]	244	274	304	
EDOT Monomer	227	256	316	436
EDOT Polymer	248		320	515

According to literature, DBCOT gives three peaks at 244, 274, and 304 nm.[65] These peaks come from the vibrations within the three aromatic rings. For the EDOT monomer, these ring vibrations are still observed at the similar wavelength values at 227, 255, and 316 nm with molar absorptivity values of 25144, 17408, and 36040 $M^{-1}cm^{-1}$ respectively. Molar absorptivity values are determined by calibration curve (*Figure 25*). However, the peak at 436 nm gives a very small intensity. A possible explanation for this peak is a charge transfer from the double bond on thiophene to the central three-ring-system. This explanation is acceptable because a charge transfer band is generally very low in intensity. To further prove this hypothesis, a solvatochromism exam can be done with a series of solvents that have different polarity values.

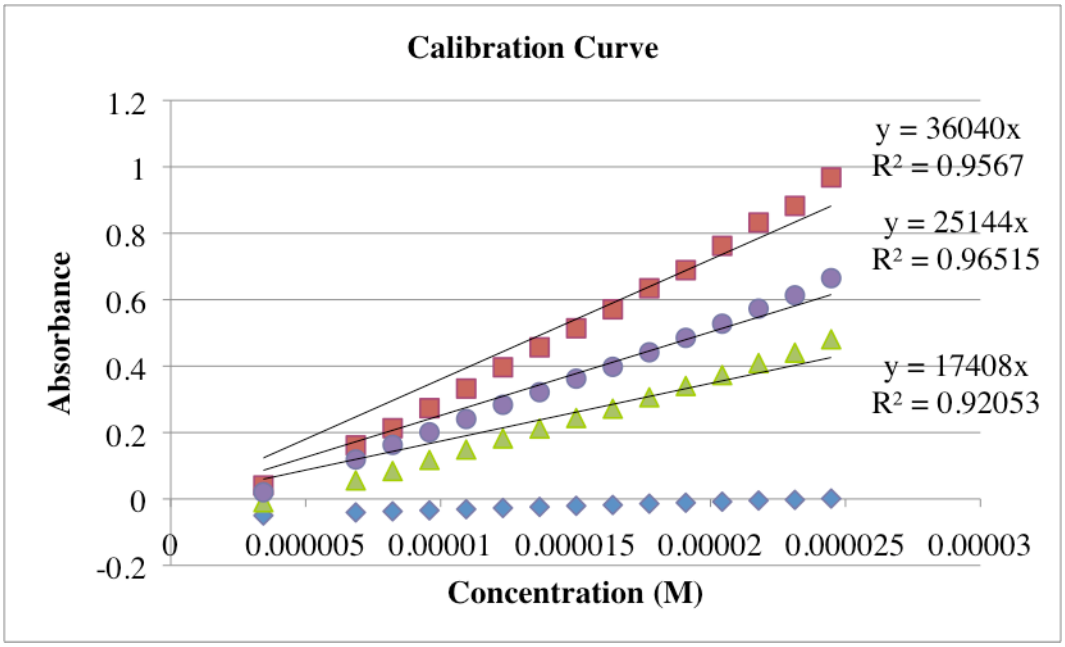

Figure 25: Calibration Curve for EDOT Monomer.

For the polymer film, three peaks are observed. Peak at 248 nm has a greater intensity than the one at 320 nm. According to the experimental result in the monomer, it is possible to hypothesize that the peaks at 227 nm and 255 nm have overlapped each other and hence are observed as one peak at 248 nm. Peak at 515 nm is thought to be the $\pi \rightarrow \pi^*$ polymer absorption.

2.5 Conclusion

A new polymer with DBCOT as its actuation center and EDOT as a polymer chain is successfully synthesized. Cyclic voltammetry method is used for the polymerization. Some properties of the EDOT monomer and polymer are similar to the DBCOT itself. The half wave potential of reduction is

approximately -0.9 V in CH_2Cl_2 and -1.2 V in ACN with a scan rate of 500 mV per second. For the EDOT monomer, a possible charge transfer from thiophene to DBCOT is found at 436 nm. For the polymer, an absorption is found at 515 nm and has been assigned as a $\pi \rightarrow \pi^*$ transition. Thickness of the polymer is also examined, but an uneven surface is obtained.

Generally speaking, this polymer can be used under a small voltage. Further improvement can be done changing the solvent to improve the polymerization and the further redox potential values can be obtained. A solvatochromism test should be done on the monomer to examine the charge transfer band in the UV-Vis absorption. The polymerization method needs to be improved so an even surface can be obtained since it is necessary for a thickness test and the corresponding conductivity test. By changing the polymer chain with other polythiophene derivatives, more properties of the DBCOT center can be obtained.

Appendix A

^{1}H NMR of 5-Bromo-2-methylbenzaldehyde

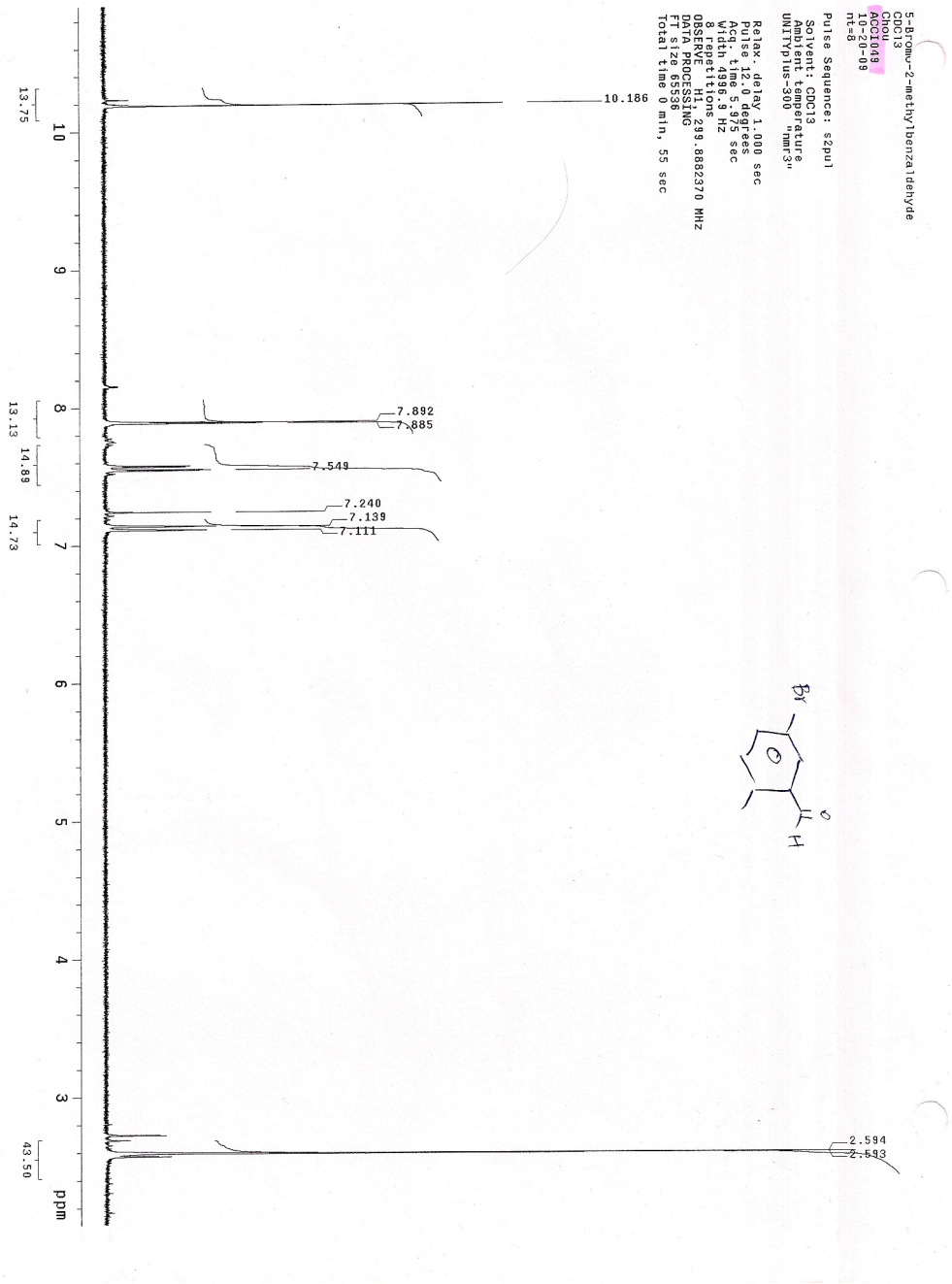

Appendix B

^{1}H NMR of 5-Bromo-2-methylbenzaldehyde, Aromatic Region

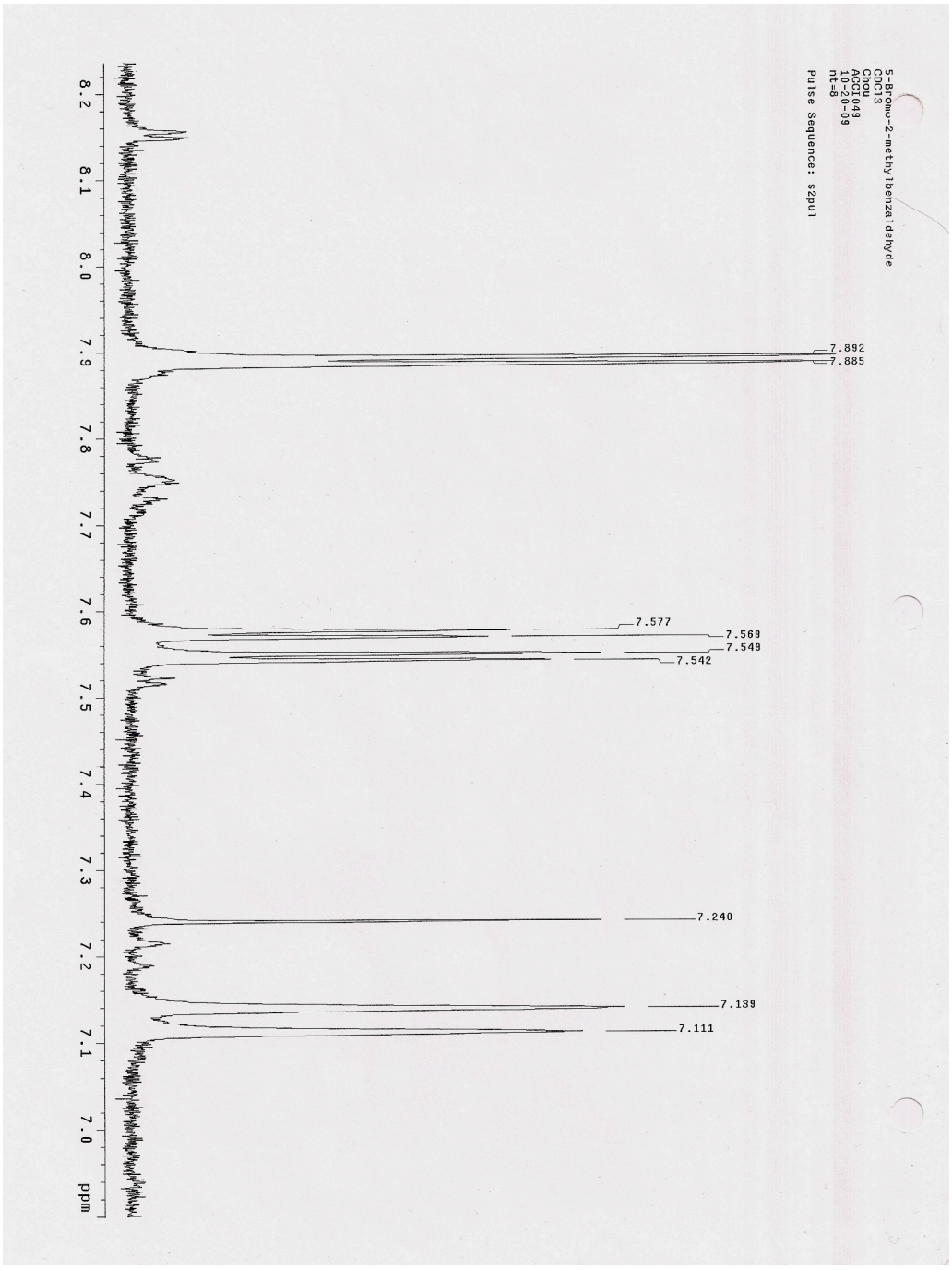

Appendix C

^{13}C {^{1}H} NMR of 5-Bromo-2-methylbenzaldehyde

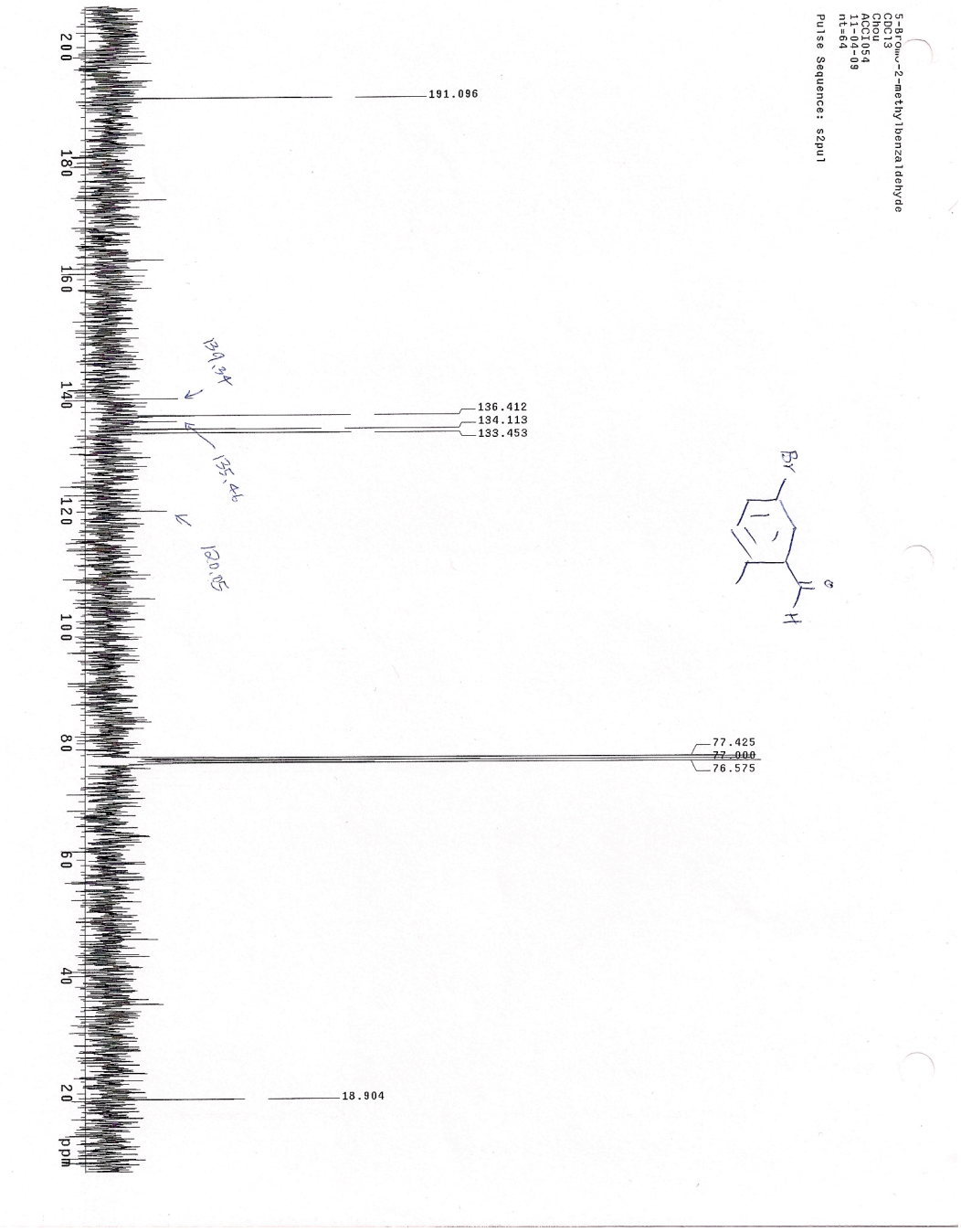

Appendix D

^{1}H NMR of 5-Bromo-2-methylphenylmethylene Diacetate

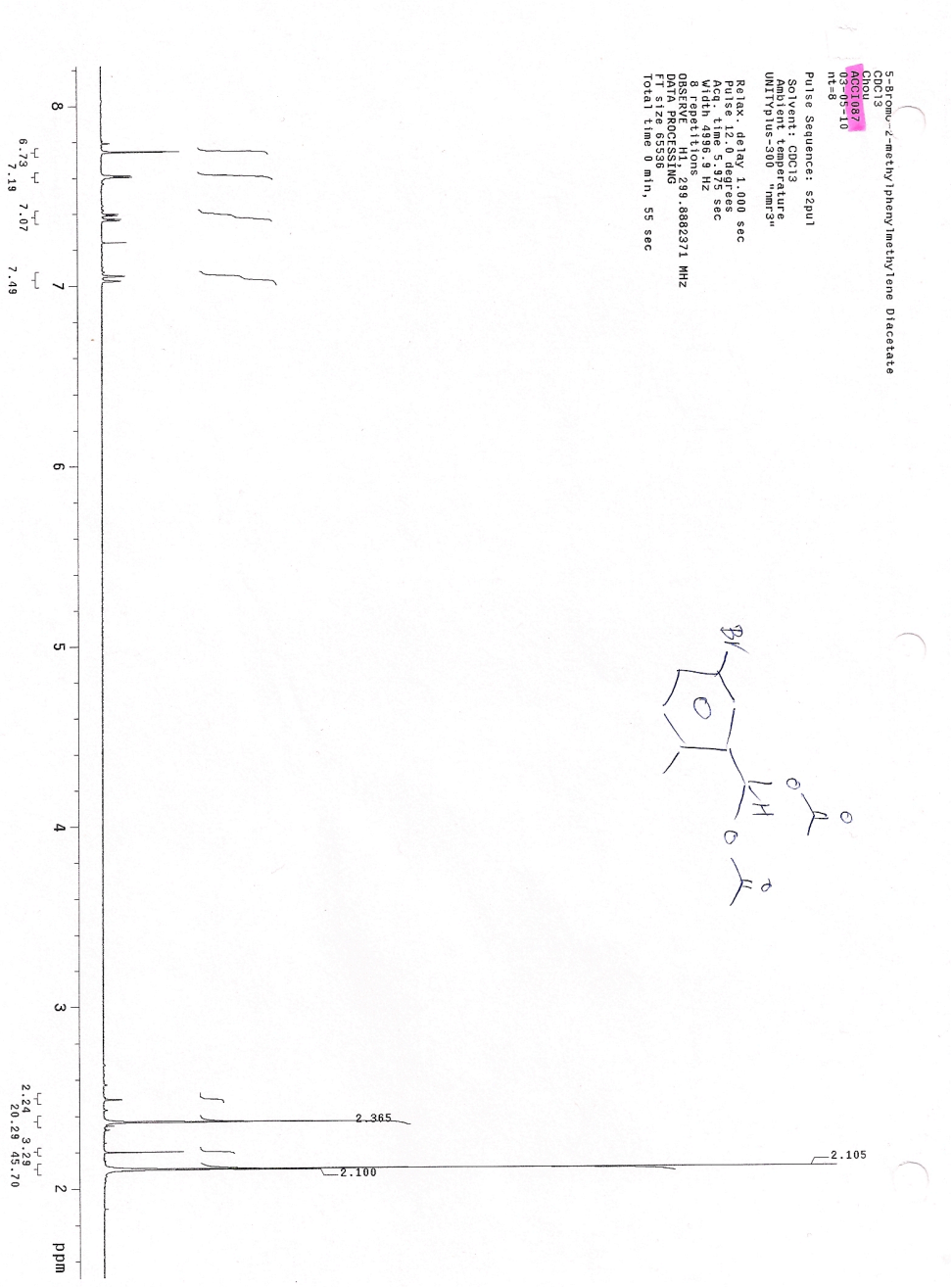

Appendix E

^{1}H NMR of 5-Bromo-2-methylphenylmethylene Diacetate, Aromatic Region

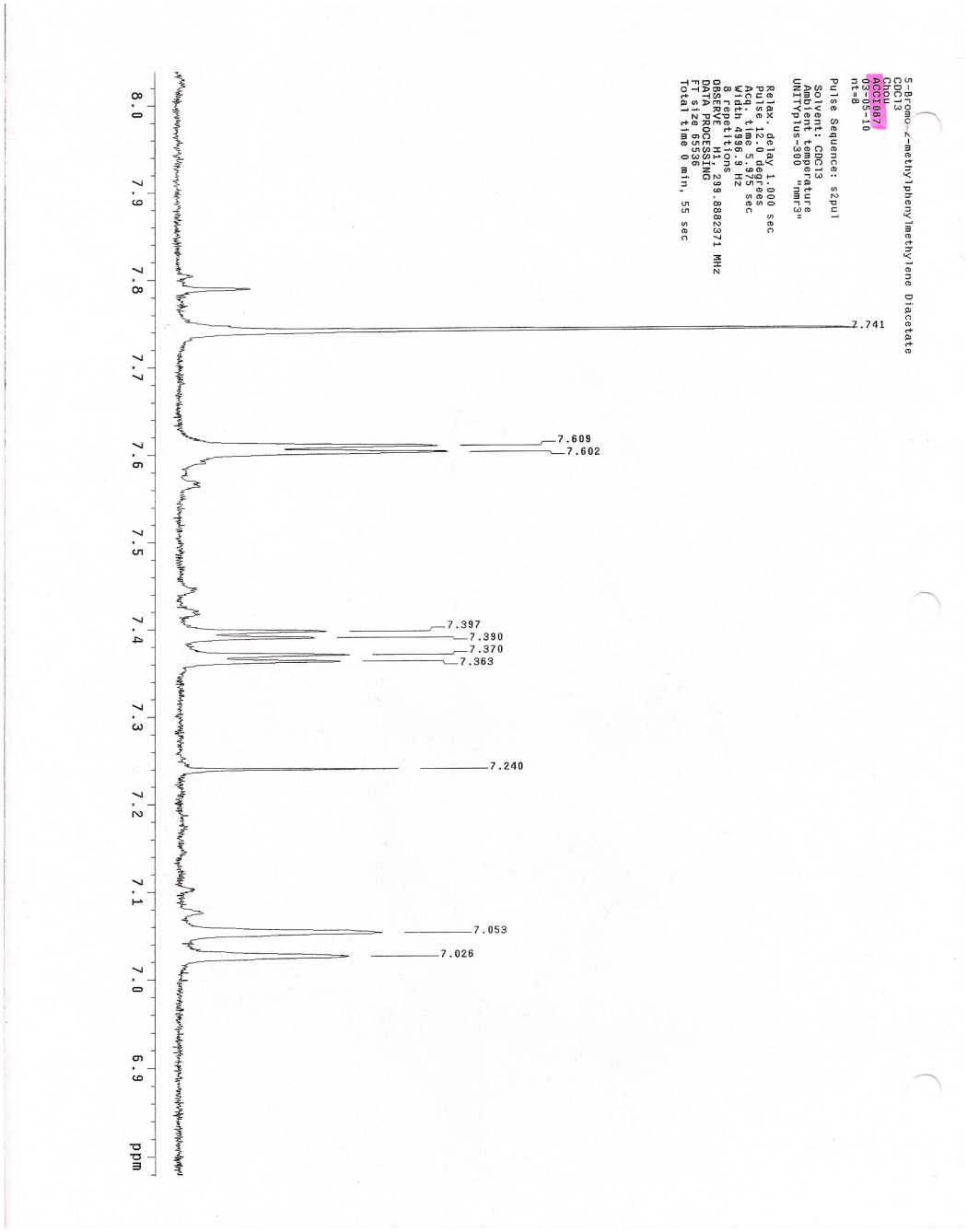

Appendix F

^{13}C {^{1}H} NMR of 5-Bromo-2-methylphenylmethylene Diacetate

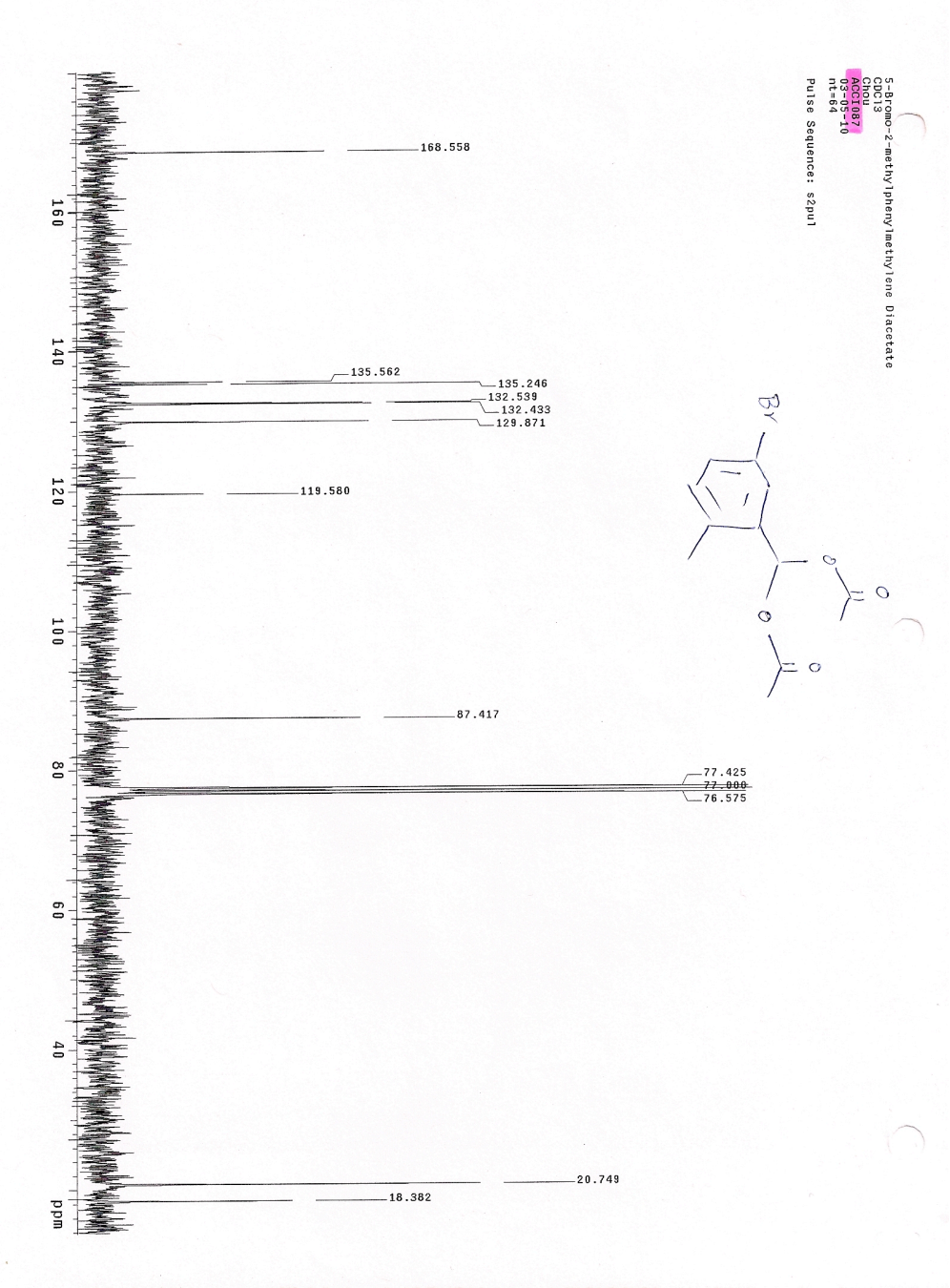

Appendix G

^{1}H NMR of 5-Bromo-2-bromomethylphenylmethylene Diacetate

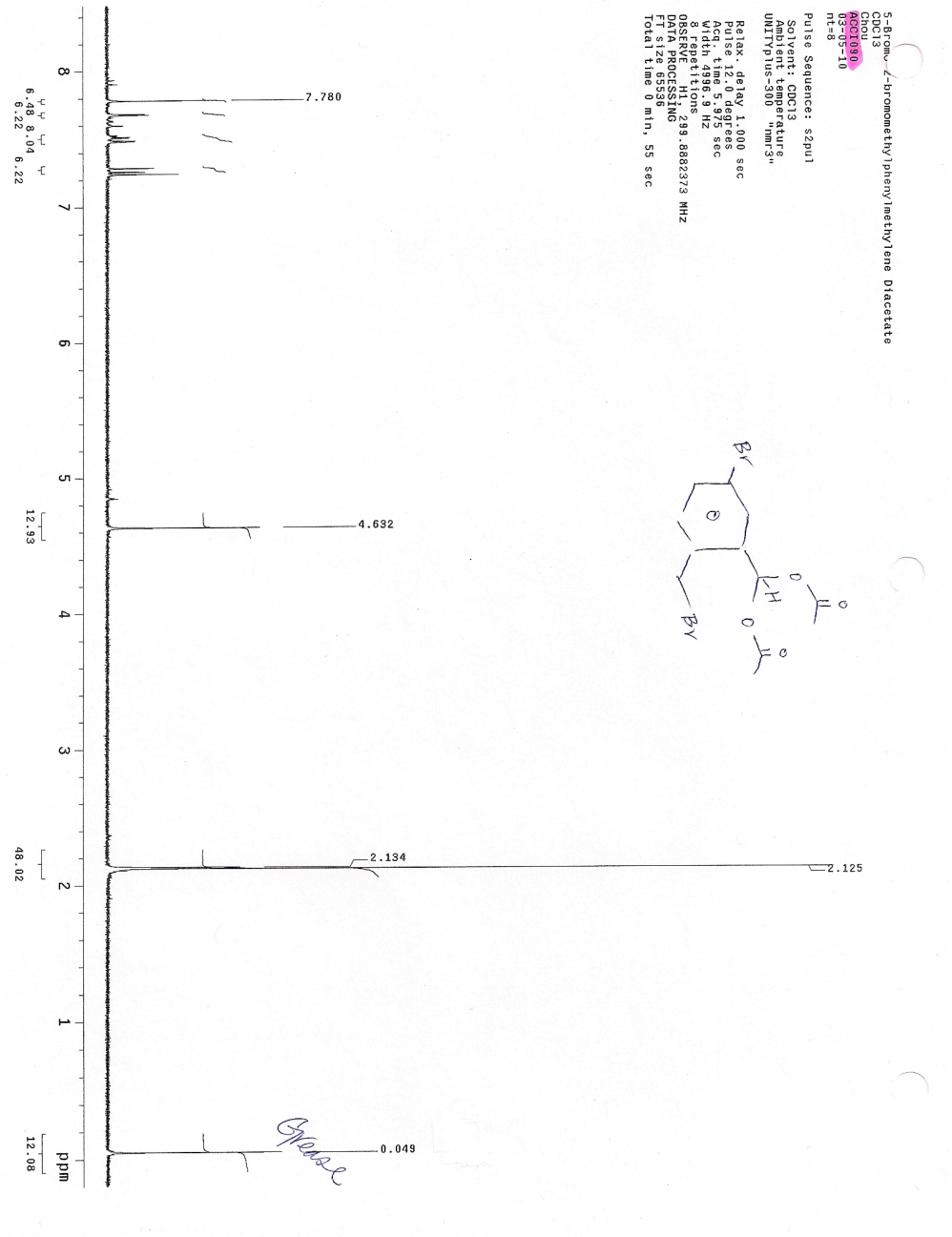

Appendix H

^{1}H NMR of 5-Bromo-2-bromomethylphenylmethylene Diacetate, Aromatic Region

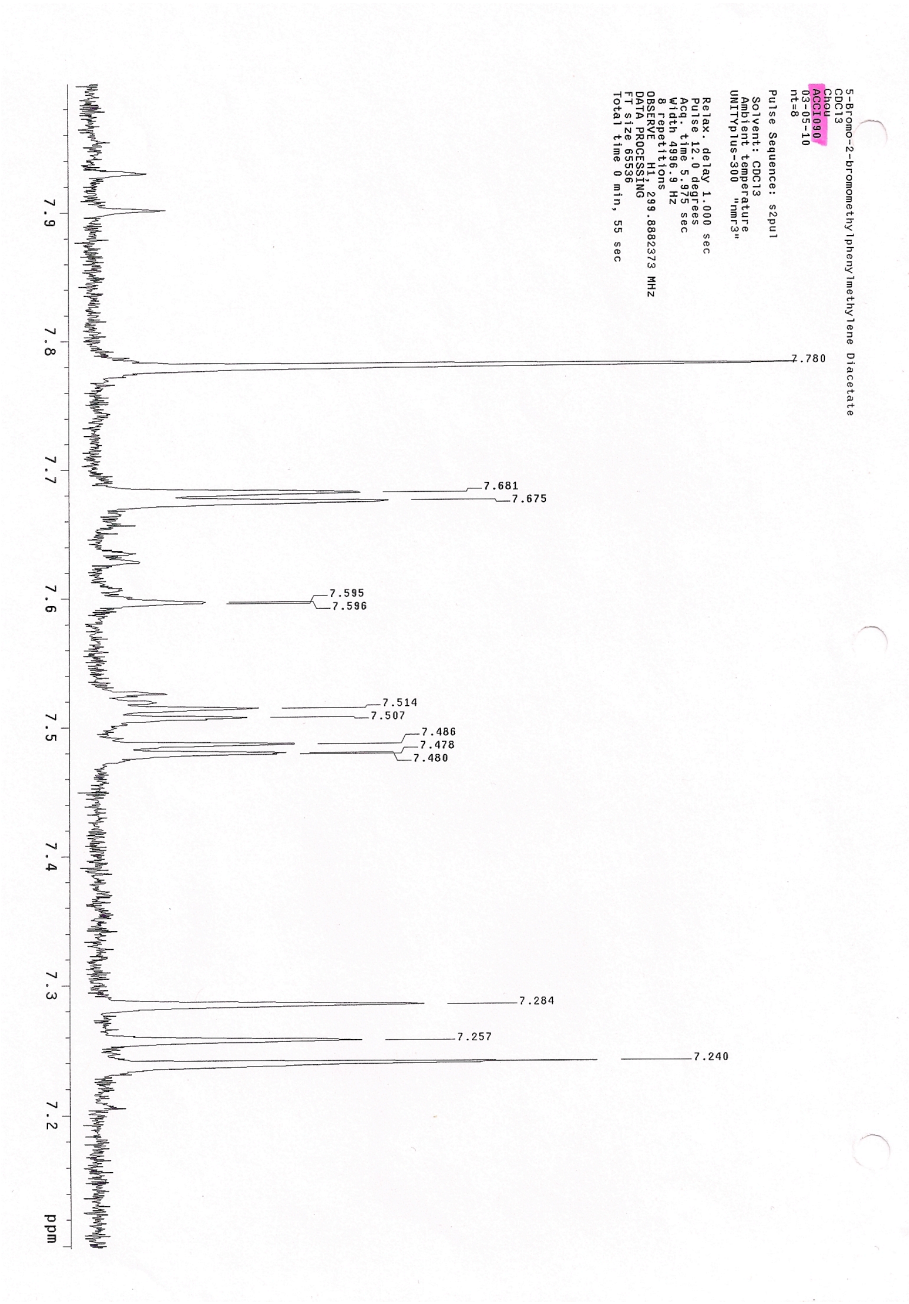

Appendix I

^{13}C {^{1}H} NMR of 5-Bromo-2-bromomethylphenylmethylene Diacetate

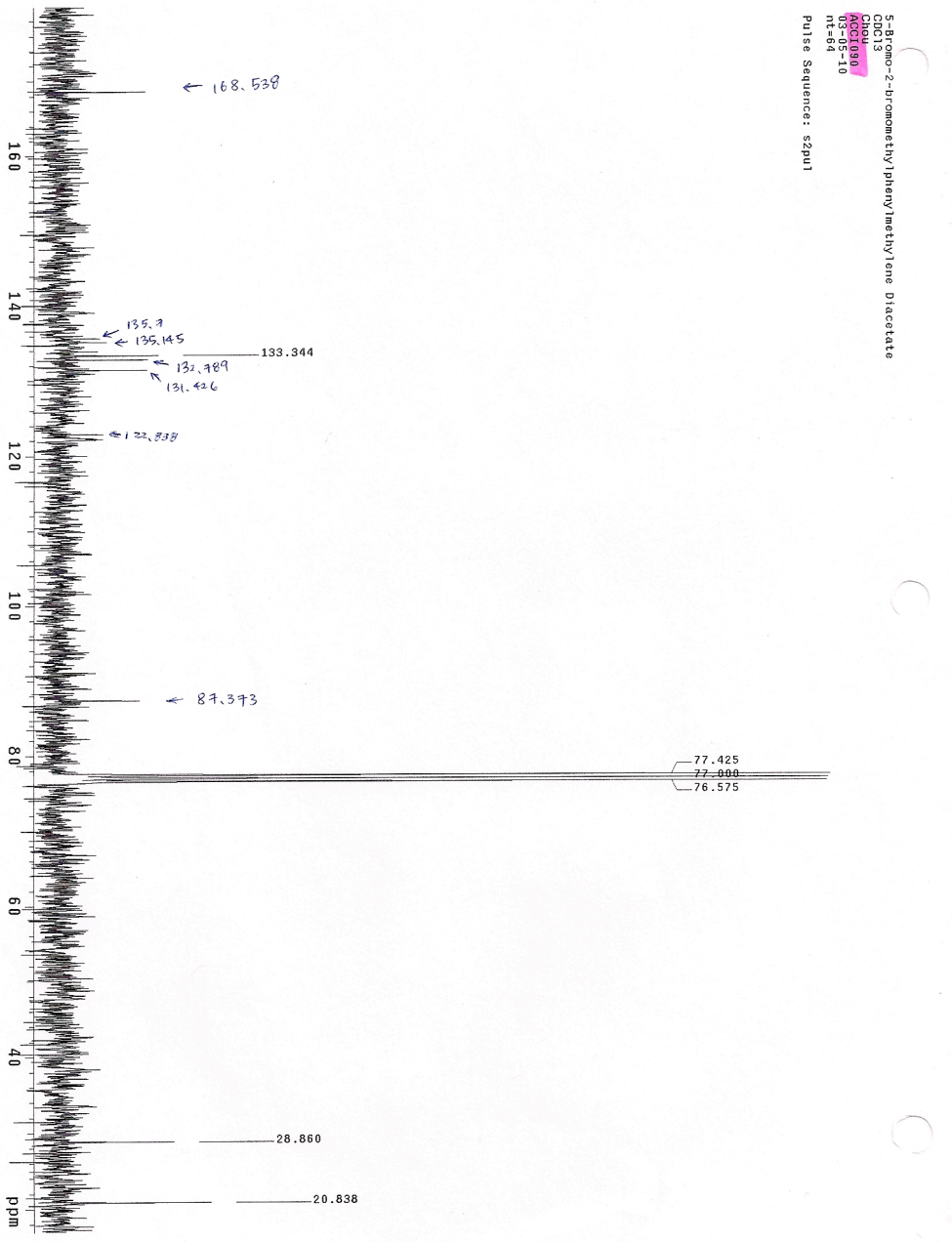

Appendix J

^{1}H NMR of (4-Bromo-2-dizcetoxymethylbenzyl)triphenylphosphonium Bromide

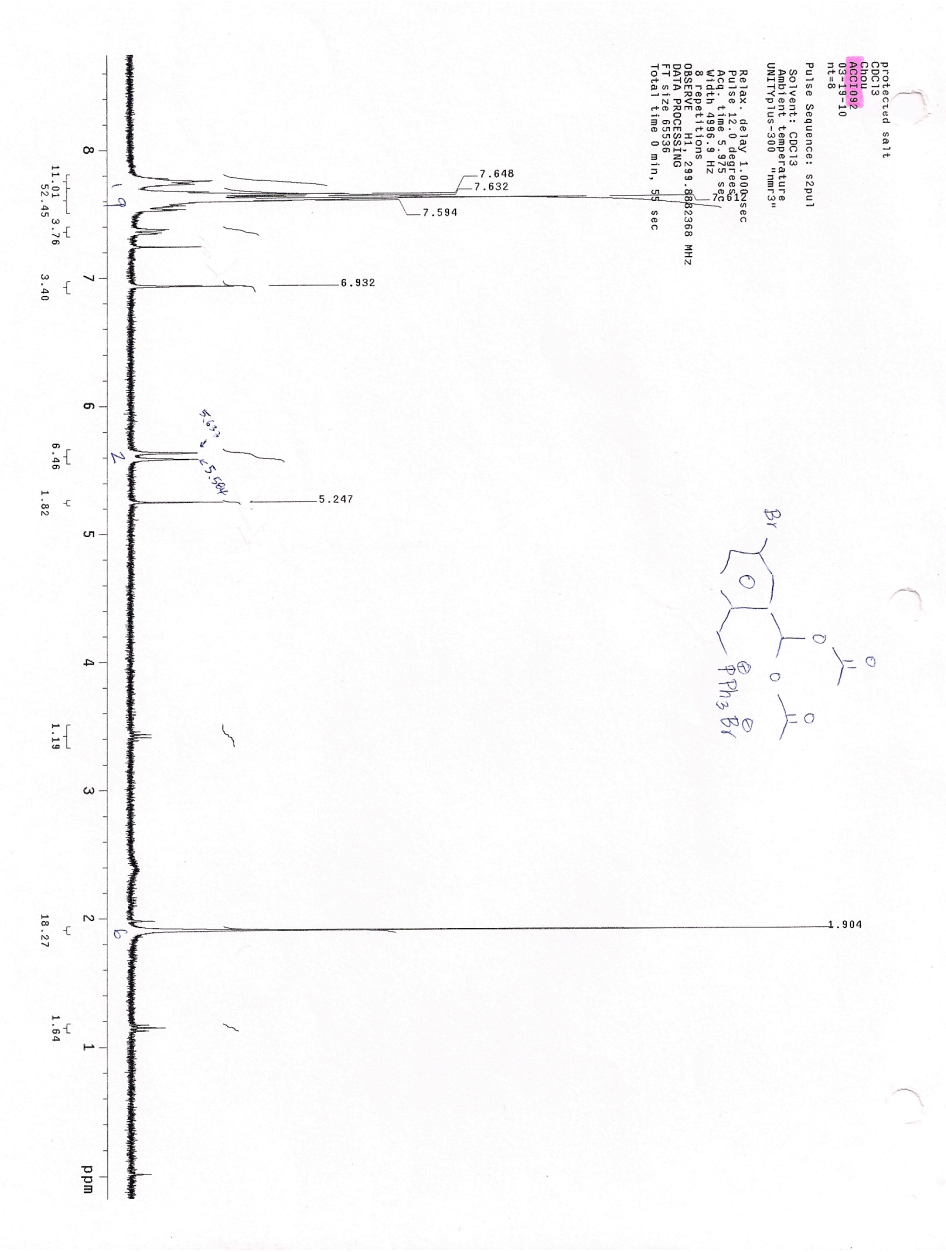

Appendix K

^{1}H NMR of (5-Bromo020fomylbenzyl)triphenylphosphonium Bromide

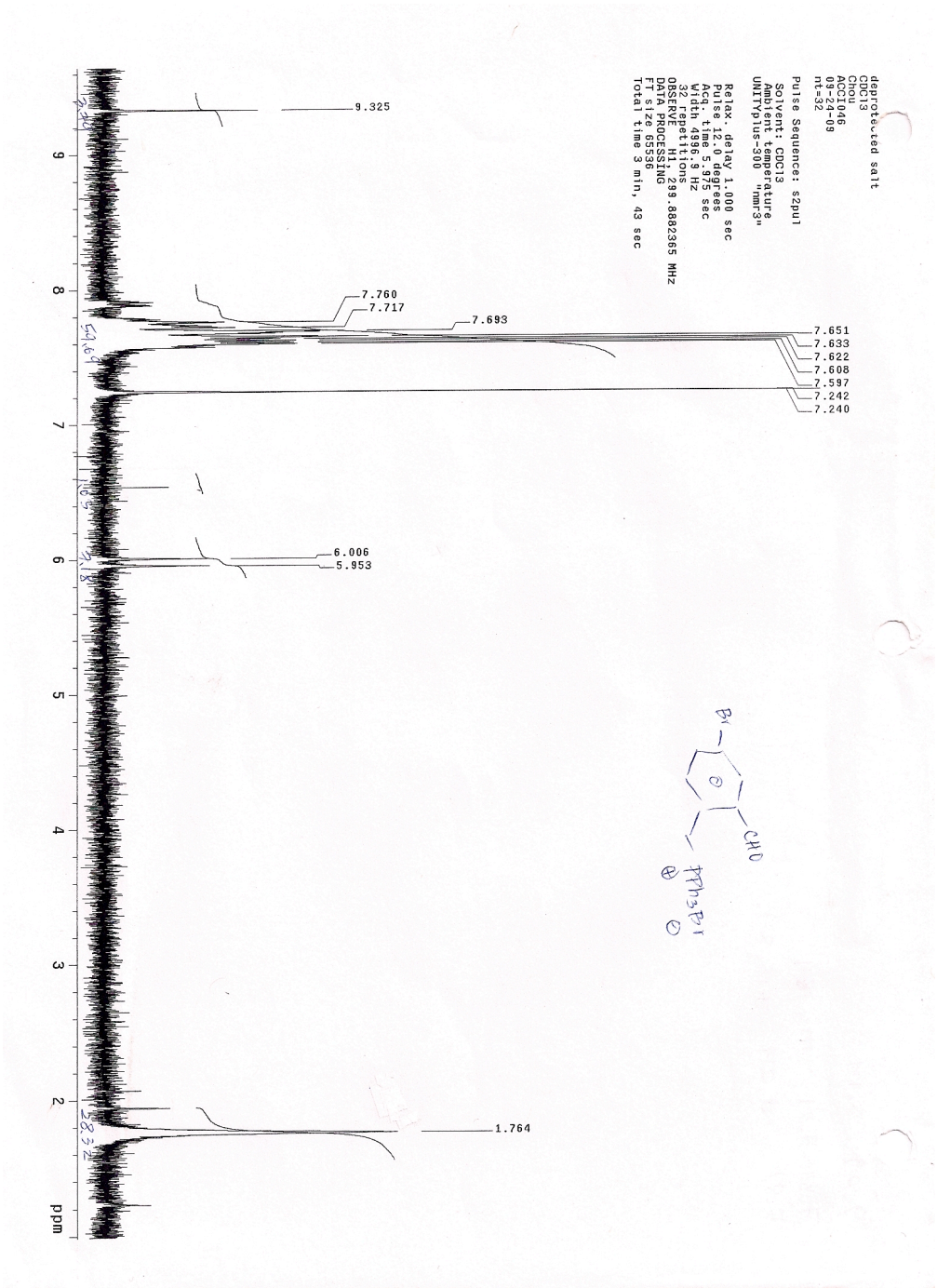

Appendix L

^{1}H NMR of 2,8-Dibromodibenzo[a,e]cyclooctatetraene

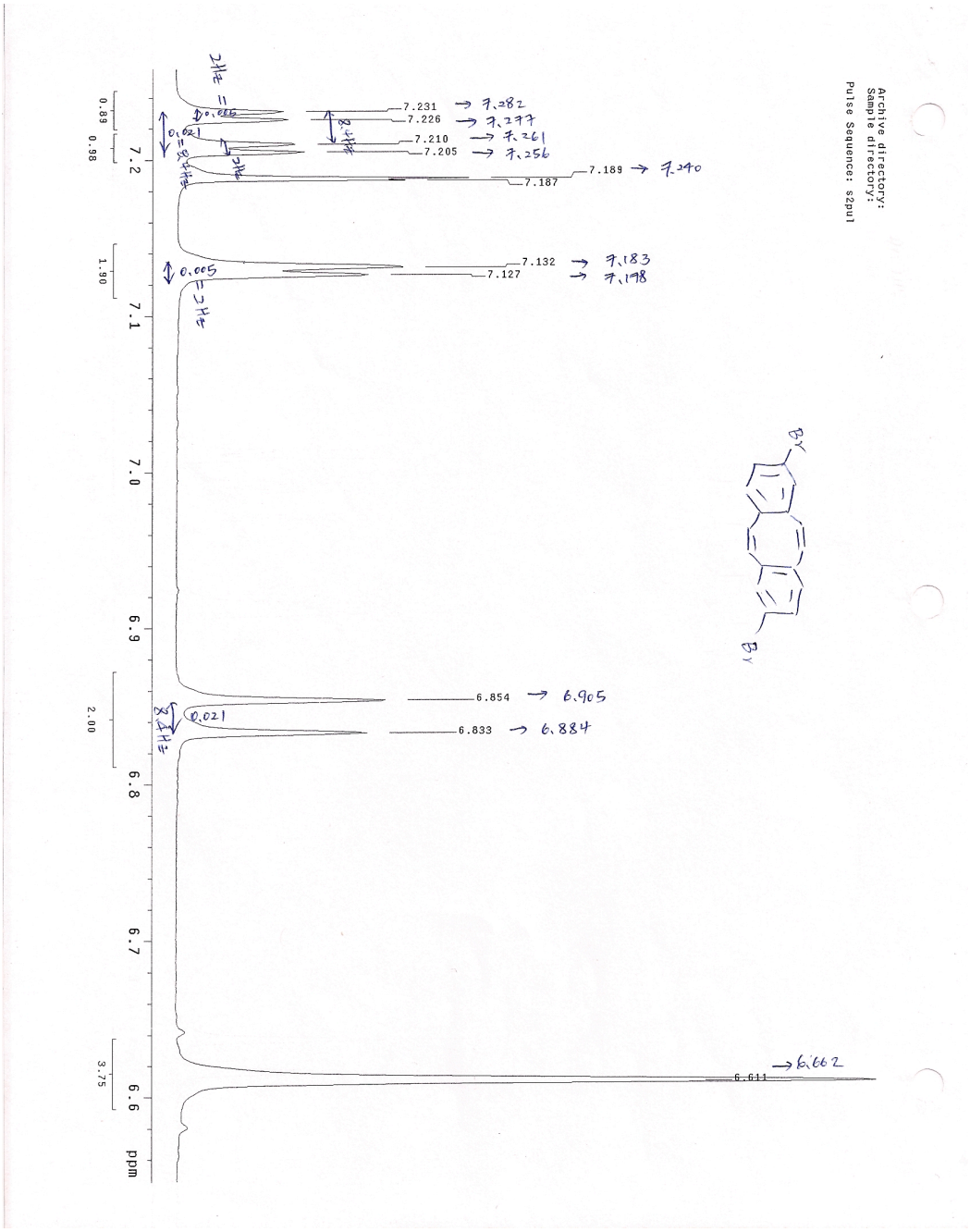

Appendix M

^{13}C {^{1}H} NMR of 2,8-Dibromodibenzo[a,e]cyclooctatetraene

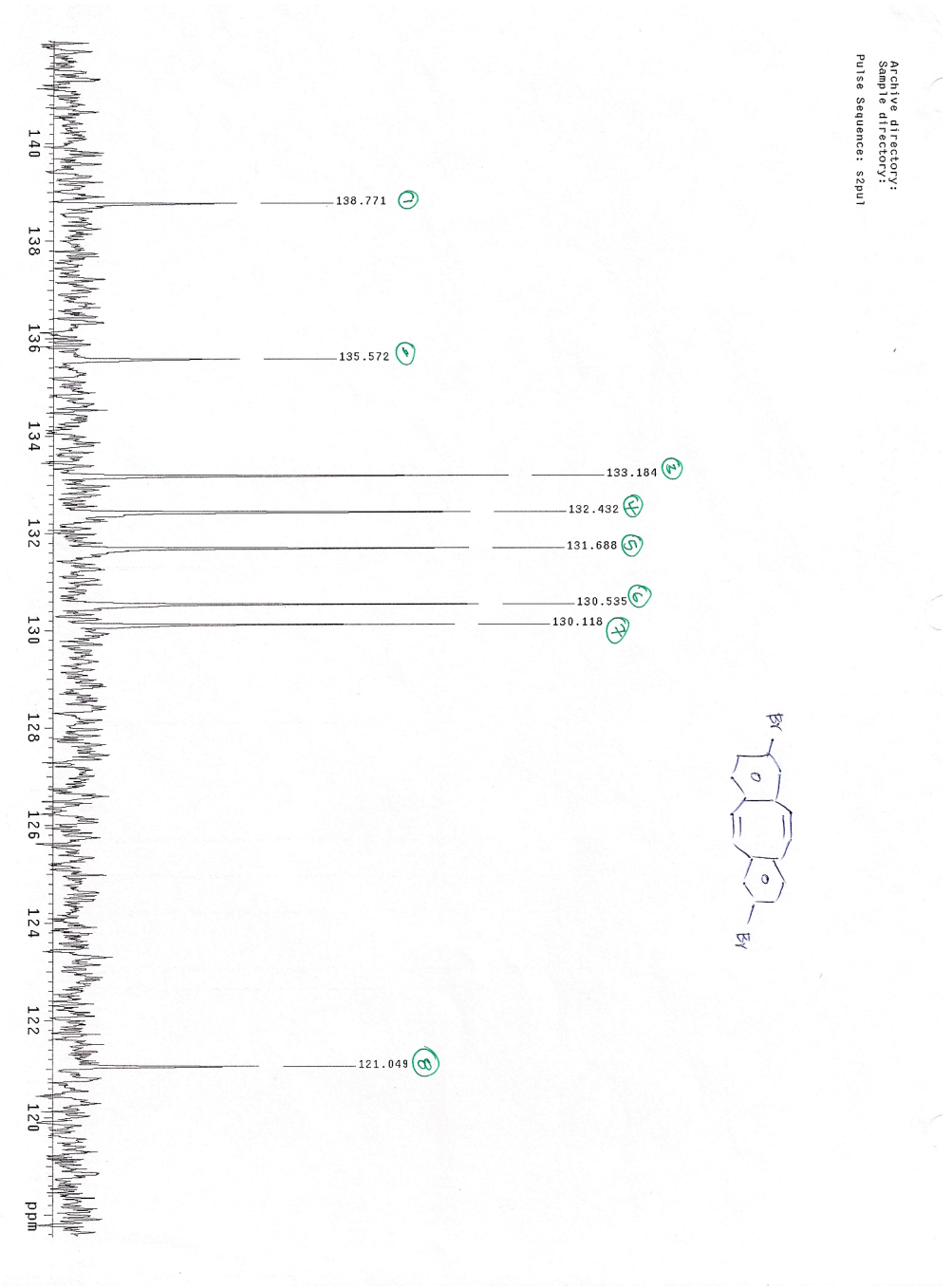

Appendix N

^{1}H NMR of 2,8-Di(3,4-ethylenedioxythiophene)dibenzo[a,e]cyclooctatetraene

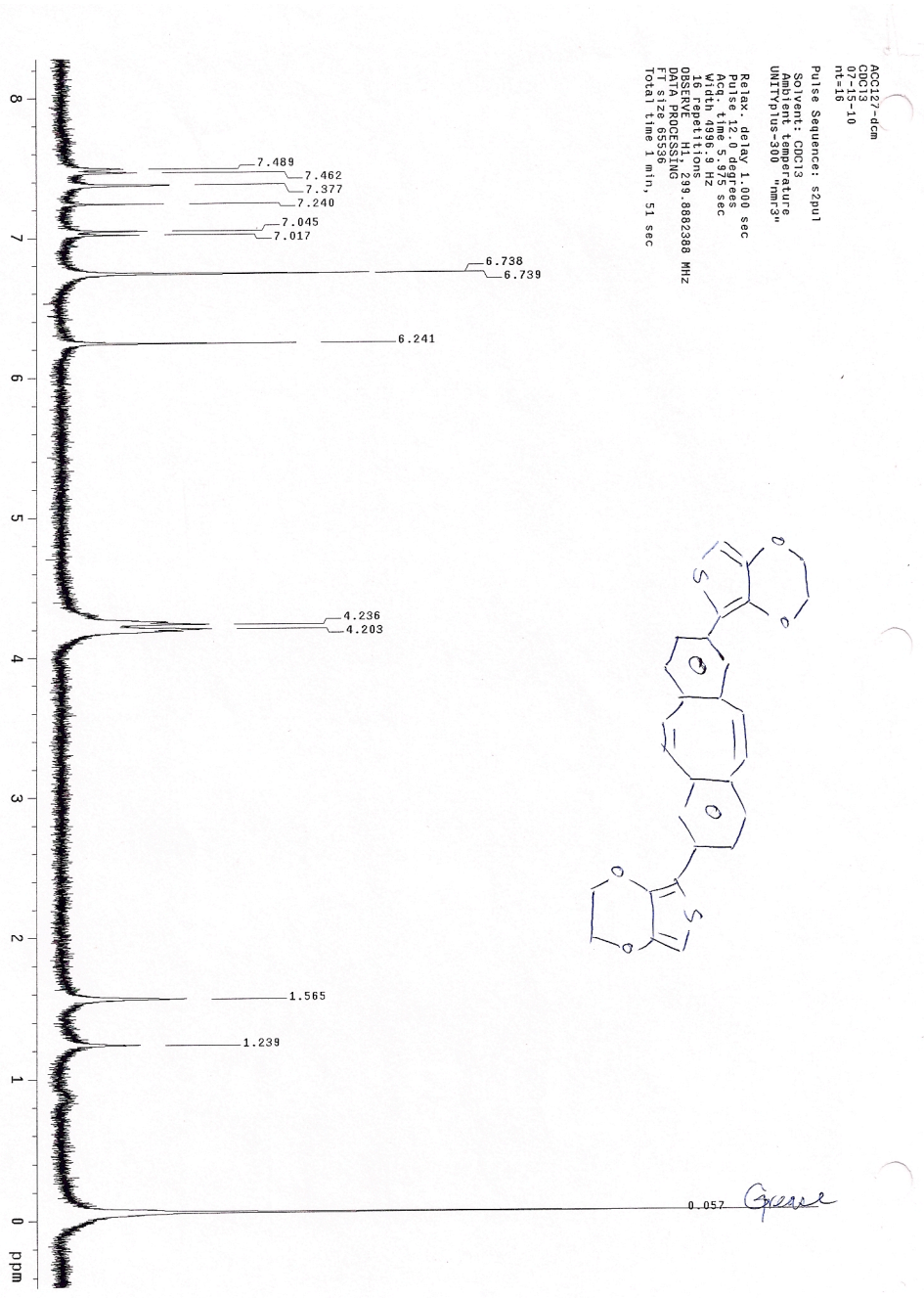

Appendix O

^{1}H NMR of 2,8-Di(3,4-ethylenedioxythiophene)dibenzo[a,e]cyclooctatetraene, Aromatic Region

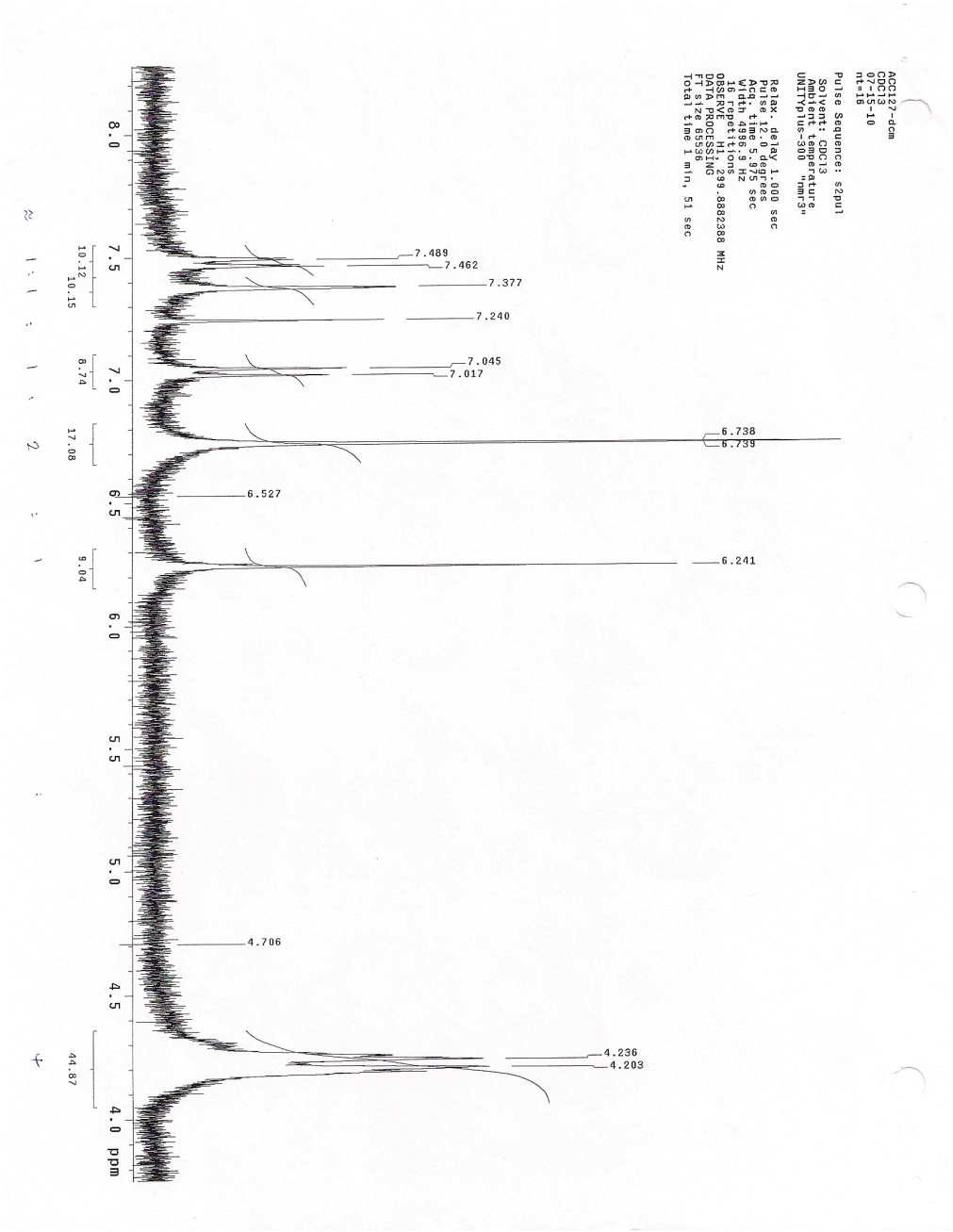

Appendix P

UV-Vis Data for Calibration Curve of Monomer

conc (µM)	conc (M)	Vstock (mL)	Vt (mL)	436	316	256	227
3.43379515	3.4338E-06	0.005	3.005	-0.04968723	0.04051185	-0.00984942	0.02027361
6.85618233	6.8562E-06	0.01	3.01	-0.04051932	0.16132127	0.05580305	0.11888522
8.22195571	8.222E-06	0.012	3.012	-0.03723719	0.21308239	0.08409217	0.1628716
9.58591651	9.5859E-06	0.014	3.014	-0.03438193	0.27336493	0.11745096	0.20076819
10.9480683	1.0948E-05	0.016	3.016	-0.03072827	0.33242804	0.14872311	0.24074848
12.3084148	1.2308E-05	0.018	3.018	-0.0271067	0.39642501	0.18212147	0.28354624
13.6669595	1.3667E-05	0.02	3.02	-0.02394906	0.45657569	0.21198565	0.32149449
15.023706	1.5024E-05	0.022	3.022	-0.02069277	0.51391441	0.24369955	0.36224216
16.3786578	1.6379E-05	0.024	3.024	-0.01808605	0.57101679	0.27180627	0.39777392
17.7318186	1.7732E-05	0.026	3.026	-0.0141568	0.63441664	0.30612749	0.44160816
19.0831918	1.9083E-05	0.028	3.028	-0.01125998	0.68902016	0.34020194	0.48508728
20.432781	2.0433E-05	0.03	3.03	-0.00822806	0.7620557	0.37293577	0.52767235
21.7805898	2.1781E-05	0.032	3.032	-0.00466431	0.83229977	0.40912077	0.57298827
23.1266216	2.3127E-05	0.034	3.034	-0.00263901	0.88225496	0.44041514	0.61310357
24.47088	2.4471E-05	0.036	3.036	0.00129423	0.96798778	0.48070809	0.66478533

Appendix Q

UV-Vis Spectrum of Polymer

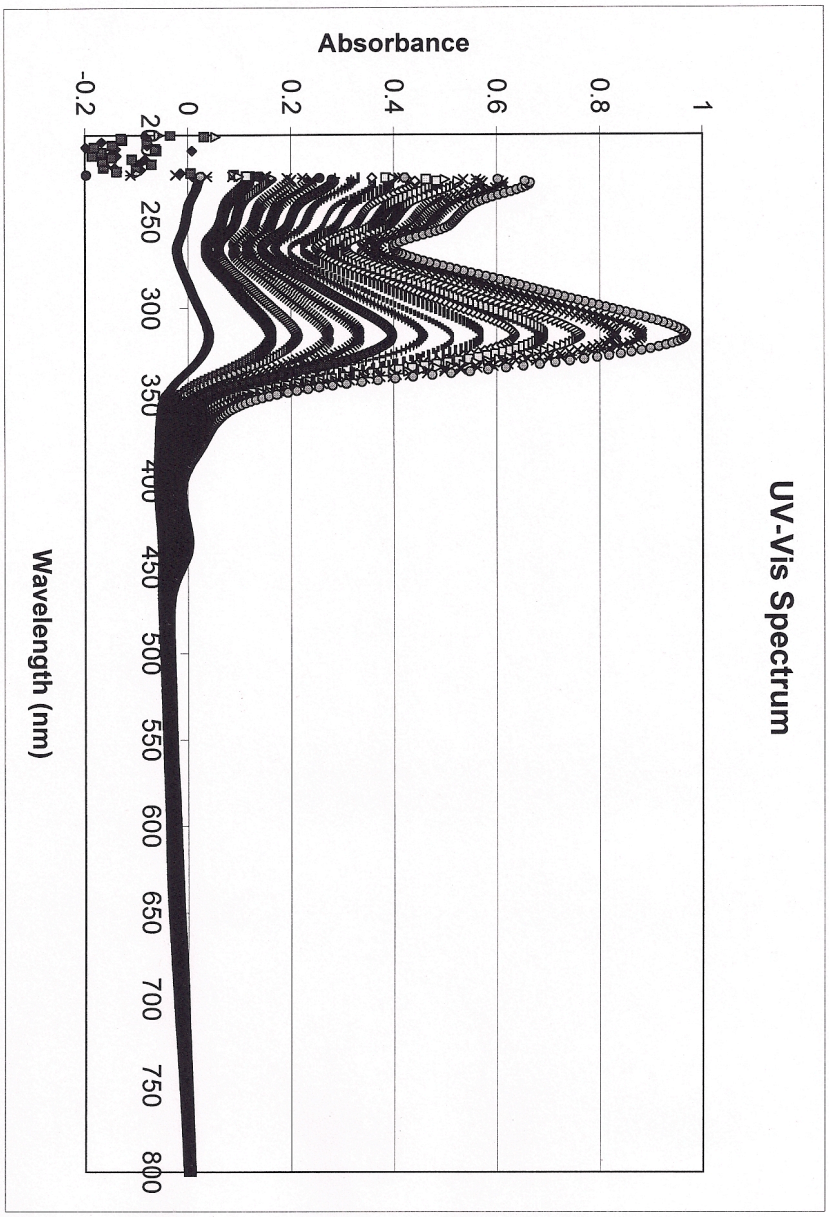

References

1. Mirfakhrai, T., Madden, J.D.W., Baughman, R.H.; *Materials Today*, 2007, 10(4), 30-38.
2. Anquetil, P.A., Yu, H., Madden, J.D., Madden, P.G., Swager, T.M., Hunter, I.W.; *Smart Structure and Materials*, 2002, EAPAD, SPIE, 4695, 424-434.
3. Ashley, S.; *Sci. Am.* 2003, Oct., 52-59.
4. Senders, C.W., Tollefson, T.T., Curtiss, S., Wong-Foy, A., Prahlad, H.; *Arch. Facial Plast. Surg.*, 2010, 12(1), 30-36.
5. Tollefson, T.T., Senders, C.W.; *Laryngoscope*, 2007, 117(11), 1907-1911.
6. Bar-Cohen, Y.; *Handbook on Biomimetics*, NTS Inc., 2000, Ch 8.
7. Pelrine, R., Kornbluh, R., Pei, Q., Stanford, S., Oh, S., Eckerle, J., Full, R., Rosenthal, M., Meijer, K.; *Smart Structure and Materials*, 2002, EAPAD, SPIE, 4695, 126-137.
8. Bar-Cohen, Y.; *Biomimetics: Biologically Inspired Technologies*, CRC Press, 2006, Ch 10.
9. Shahinpoor, M., Kim, K.J., Majarrad, M.; *Artificial Muscles: Application of Advanced Polymeric Nanocomposites*, Taylor & Francis Group, LLC, CRC Press, 2007, Ch 1.

10. Oter, T.F., Grande, H., Rodriguez, J.; *J. Electrical Chem*., 1995, 394, 211-216.

11. Li, F.K., Zhu, W., Zhang, X., Zhao, C.T., Xu, M.; *J. Appl. Polym. Sci*., 1999, 71(7), 1063-1070.

12. Chou, C.P., Hannaford, B.; *IEEE Intl. Conf. on Robotics and Automation*, IEEE, San Diego, CA, May, 1994, 1, 281-286.

13. Zrinyi, M., Barsi, L., Szabo, D., Kilian, H.G.; *J. Chem. Phys*., 1997, 106(13), 5685-5692.

14. van der Veen, G., Prins, W.; *Phys. Sci*., 1971, 230, 70.

15. Katchalsky, A.; *Experientia*, 1949, V, 319-320.

16. Tobushi, H., Okumura, K., Hayashi, S., Ito, N.; *Mechanics of Materials*, 2001, 33(10), 545-554.

17. Yu, Y., Nakano, M., Ikeda, T.; *Nature*, 2003, 425, 145.

18. Rontgen, W.C.; *Ann. Phys. Chem*., 1880, 11, 771-786. (In German).

19. Kepling, C., Kaltenbrunner, M., Arnold, N., Bauer, S.; *PNAS*, 2010, 107(10), 4505-4510.

20. Sacerdote, M.P.; *J. Phys*., 1899, VIII (3, series t), 31.

21. Eguchi, M.; *Phil. Mag*., 1925, 49, 178-192.

22. Fukada E.; *IEEE Transactions on Ultrasonics, Ferroelectrics, and Frequency Control*, 2000, 47(6), 1277-1289.

23. Takamatsu, T., Sumoto, I.; *Riken Hokoku*, 1969, 45, 141-148. (In Japanese).

24. Mark, J.E.; *Physical Properties of Polymers Handbook, 2nd ed*, Springer Science, Business Media, LLC, 2007, Ch 48.4.

25. Zhang, Q.M., Bharti, V., Zhao, X.; *Science*, 1998, 280, 2101-2104.

26. Clark, R.K.; *Anatomy and Physiology: Understanding the Human Body,* Jones and Bartlett Publisher, Inc., 2005, Ch. 9.

27. Nelson, D.L., Cox, M.M.' *Lehninger Principles of Biochemistry, 4th ed*, W. H. Freeman and Company, 2005, Ch 5.

28. Lai, S., Elliot, D.; *Surg*, 2007, 1(1), 3-14.

29. Cooper, G.M.; *The Cell, A Molecular Approach, 2nd ed*., Sinauer Associates, 2000, Ch 11.

30. Collin, J-P., Dietrich-Buchecker, C., Garina, P., Jimenez-Molero, M.C., Sauvage, J-P.; *Acc. Chem. Res*., 2001, 34,6,477-487.

31. Jimenez, M.C., Dietrich-Buchecker, C., Sauvage, J-P.; *Angew. Chem. Int. Ed*., 2000, 39,18,3284-3287.

32. Bar-Cohen, Y.; *Electroactive Polymer (EAP) Actuators as Artificial Muscles, 2nd edition*, SPIE Press, 2004.

33. Perline, R., Kornbluh, R., Pei, Q., Joseph, J.; *Science*, 2000, 287, 836-839.

34. Camacho-Lopez, M., Finkelmann, H., Palffy-Muhoray, P., Shelley, M.; *Natural Materials*, 2004, 3, 307-310.

35. Baughman, R.H., Zakhidov, A.A., de Heer, W.A.; *Science*, 2002, 297, 787-792.

36. Baughman, R.H., Cui, C., Zakhidov, A.A., Iqbal, Z., Barisci, J.N., Spinks, G.M., Wallace, G.G., Mazzoldi, A., De Rossi, D., Rinzler, A.G., Jaschinski, O., Roth, S., Kertesz, M.; *Science*, 1999, 284, 1340-1344.

37. Endo, M., Hayashi, T., Kim, Y.A., Terrones, M., Dresselhaus, M.S.; *Phil. Trans. R. Soc. Lond. A*, 2004, 362, 2223-2238.

38. Spudich, J.A.; *Nature*, 1994, 372, 515-518.

39. Inzett, G.; *Conducting Polmers: Monographs in Electrochemistry*, Springer, 2008, Ch 8.

40. Baughman, R.H.; *Synthetic Metals*, 1996, 78, 339-353.

41. Letheby, H.; *J. Chem. Soc.*, 1862, 15, 161.

42. Bott, D.; *Phys. Technol.*, 1985, 16, 121.

43. *Shahinpoor, M.,* Kim, K.J., Majarrad, M.; *Artificial Muscles: Application of Advanced Polymeric Nanocomposites*, Taylor & Francis Group, LLC, CRC Press, 2007, Ch 8.

44. Nobelprize.org; *The Nobel Prize in Chemistry 2000*, 2000, http://nobelprize.org/nobel_prizes/chemistry/laureates/2000/

45. Baughman, R.H., Shacklette, L.W., Elsendaumer, R.L., Plichta, E.J., Becht, C.; *Molecular Electronics*, Kluwer Academic Publisher, 1991.

46. Otero, T.F., Sansinena, J.M.; *Bioelectrochem. Bioenergetics*, 1995, 28, 411-414.

47. Otero, T.F., Sansinena, J.M.; *Adv. Mater.*, 1998, 10(6), 491-494.

48. Della Santa, A., De Rossi, D., Mazzoldi, A.; *Smart Mater. Struct.*, 1997, 6, 23-24.

49. De Rossi, D., Suzuk, M., Osada, Y., Morasso, P.; *J. Intelligent Mater. Syst. Struct.*, 1992, 3, 75-95.

50. Mislow, K., Perlmutter, H.D.; *J. Am. Chem. Soc.*, 1962, 84(18), 3591-3592.

51. Graham Solomons, T.W., Fryhle, C.B.; *Organic Chemistry, 8th ed*, John Wiley & Sons, Inc., 2004, Ch 14.7.

52. Marsella, M.J., Reid, R.J., Estassi, S., Wang, L.; *J. Am. Chem. Soc.*, 2002, 124(42), 12507-12510.

53. Kojima, H., Bard, A.J., Wong, H.N.C., Sondheimer, F.; *J. Am. Chem. Soc.*, 1976, 98(18), 5560-5565.

54. Gerson, F., Felder, P., Schmidlin, R., Wong, H.N.C.; *J. Chem. Soc., Chem. Commun.*, 1994, 1659-1660.

55. Bachrach, S.M.; *J. Org. Chem.*, 2009, 74(9), 3609-3611.

56. Chiang, C.K., Fincher, C.R., Jr., Park, Y.W., Heeger, A.J., Shirakawa, H., Lois, E.J., Gau, S.C., MacDiarmid, A.G.; *Phys. Rev. Lett.*, 1988, 39, 1098.

57. Schopf, G., Kobmehl, G.; *Polythiophenes – Electrically Conductive Polymers*, Springer – Verlag Berlin Heidelberg, 1997.

58. Karpfen, A., Kertesz, M.; *J. Phys. Chem.*, 1991, 95, 7680-7681.

59. Wallace, G.G., Spinks, G.M., Kane-Maguire, L.A.P., Teasdale, P.R., *Conductive Electroactive Polymers: Intelligent Polymer System, 3rd ed.*, CRC Press, Taylor & Francis Group, LLC, 2009, Ch 6.

60. Beck, F., Barsh, U., Michaelis, R.; *J. Electroanal. Chem.*, 1993, 55, 1272.

61. Faid, K., Cloutier, R., LeClere M.; *Synth. Met.*, 1993, 58, 295.

62. Krische, B., Zagorska, M., Hellberg, J.; *J. Am. Chem. Soc.*, 2000, 122. 29.

63. Kelly, T.R., Silva, R.A., De Silva, H., Jasmin, S., Zhao, Y.; *J. Am. Chem Soc*., 2000, 122, 29.

64. Brown, C., Sargent, M.V.; *J. Chem. Soc. C*, 1969, 1818.

65. Esser, B., Rominger, F., Gleiter, R.; *J. Am. Chem. Soc*., 2008, 130, 6716.